This document was prepared for the ETI by third parties under contract to the ETI. The ETI is making these documents and data available to the public to inform the debate on low carbon energy innovation and deployment.

Programme Area: Marine

Project: PerAWAT

Title: Report on Responses and Power Take-Off from Controlled Devices in Regular Waves

Abstract:

This report presents and discusses the results of fully nonlinear simulations of linear and nonlinear power take-off for controlled devices in regular wave interactions involving a single truncated cylinder (representing a wave energy device) and an array of four devices. By including nonlinear control and power take-off (PTO) in the device motion, the simulations here model more complex interactions. The key objectives of this study were to demonstrate the capability of OXPOT in modelling linear and nonlinear PTO mechanisms – in later deliverables involving validation of the models by comparison with experiment it will be necessary to be able to simulate the experimental setup as closely as possible. The PTO force to be used in the experiments has been specified to be nonlinear in nature. Furthermore, an investigation into the effect of nonlinearities in PTO forces and the influence of different control strategies on device response and device power take-off is conducted in this report. It outlines how these objectives have been met and describes any issues arising from their completion. The analysis of the effects of the nonlinear PTO forces is conducted using the linear PTO force results as a frame of reference. Furthermore, the results of the single device PTO simulations are utilised in the analysis of the power absorption properties of the devices in a square array.

Context:

The Performance Assessment of Wave and Tidal Array Systems (PerAWaT) project, launched in October 2009 with £8m of ETI investment. The project delivered validated, commercial software tools capable of significantly reducing the levels of uncertainty associated with predicting the energy yield of major wave and tidal stream energy arrays. It also produced information that will help reduce commercial risk of future large scale wave and tidal array developments.

Energy Technologies Institute

PerAWaT MA1003

WG1 WP1 D10: Report on responses and power take-off from controlled devices in regular waves

Author: C. Fitzgerald

Checked by: P. H. Taylor and R. Eatock Taylor

Date: 30th March 2012

Version 1.0

CONTEXT

This report (WG1 WP1 D10) presents and discusses the results of fully nonlinear simulations of linear and nonlinear power take-off for controlled devices in regular wave interactions involving a single truncated cylinder (representing a wave energy device) and an array of four devices. By including nonlinear control and power take-off in the device motion, the simulations here model more complex interactions than in WG1 WP1 D9 where the uncontrolled responses of truncated cylinders were considered. The fully nonlinear hydrodynamic model and the numerical method to solve nonlinear wave-structure interactions are described in detail in WG1 WP1 D7 and summarised in WG1 WP1 D9 and are not repeated here.

The key objectives of this study are to demonstrate the capability of OXPOT in modelling linear and nonlinear power take-off mechanisms – in later deliverables involving validation of the models by comparison with experiment it will be necessary to be able to simulate the experimental setup as closely as possible. The power take-off (PTO) force to be used by QUB in the experiments has been specified to be nonlinear in nature. Furthermore, an investigation into the effect of nonlinearities in PTO forces and the influence of different control strategies on device response and device power take-off is conducted in this report. The report outlines how these objectives have been met and describes any issues arising from the completion of these objectives. The analysis of the effects of the nonlinear power take-off forces is conducted using the linear PTO force results as a frame of reference. Furthermore, the results of the single device PTO simulations are utilised in the analysis of the power absorption properties of the devices in a square array.

TABLE OF CONTENTS

1 INTRODUCTION

1.1 Scope of this document

The implementation of power take-off and control terms in the fully nonlinear potential flow solver OXPOT allows us to model the fully nonlinear heave responses and power take-off from controlled axisymmetric devices in regular incident waves. This report considers the effects of linear and nonlinear power take-off forces on the heave response of a device and the influence of different control strategies on the power take-off capabilities of devices.

This report is divided into three main sections. In order to provide a context to the various control strategies and power take-off forces used in the simulations it was considered useful to give a brief overview of wave energy converter (WEC) power take-off and control theory in section 2. The results of the single device power take-off simulations involving linear and nonlinear PTOs are presented in section 3 and section 4 contains the results of the power take-off simulations for a square array of four devices.

The description of the WEC power take-off and control theory provided in section 2 summarises the most relevant aspects of the theory presented in section 3.6.2 of the methodology report WG1 WP1 D1B. For the sake of simplicity, the power take-off for a single heaving axisymmetric device is considered and the underlying hydrodynamic model assumes linear regular waves. This approach allows us to identify the different factors which influence power take-off (e.g. system inertia, natural frequency of the device, incident wave frequency) and to derive the fundamental conditions for optimal power absorption. The implication of the resonance or phase condition provides the basis for the discussion of two different phase control strategies – optimal reactive control and sub-optimal discrete control – that are simulated using OXPOT. A qualitative summary of discrete latching control is also included to provide a basis for the analysis of the latching simulations presented later in the report. The power take-off and control forces in the *frequency domain* description of power take-off must be linear in nature; however, in *time domain* simulations modelling the linear or fully nonlinear hydrodynamics it is straightforward to model nonlinear or discontinuous applied forces also. A wide variety of PTO mechanisms and control strategies can thus be modelled using OXPOT and a discussion of the specific nonlinear PTO force of interest is also provided in Section 2.

In Section 3, the OXPOT simulation results for the operation of a single heaving device in isolation in regular incident waves are presented. Rather than exhaustively analysing the different PTO force/control strategy combinations, a selection of cases was selected for simulation in order to understand the effect of the forces and strategies on the motion of the device and the power absorbed by the device. Particular emphasis is given to comparisons of device response and power capture for devices subject to linear and Coulomb damping PTO forces with similar steady-state amplitudes. Given that the device response settles to steady-state oscillations significantly faster when subject to PTO damping and when not operating at resonance, many of the linear and nonlinear PTO force comparative simulations are without phase control (which is used to satisfy the so-called 'resonance condition'). For the incident wave of period 9 seconds and wave height 4m, the comparisons revealed strong similarities in the amplitude and periodic form of the device responses

but significant differences in the periodic form of the instantaneous power absorption signals. However, in the case of the incident wave of period 15 seconds, the non-linear PTO force with approximately equivalent amplitude to the linear steady state PTO force introduces strong nonlinearities to the periodic response of the device.

The operation of the isolated device at resonance is also investigated with optimal reactive and sub-optimal phase control. Over the duration of the simulations (typically 20 periods), the device oscillations steadily increase but do not reach the large steady-state amplitude predicted by linear theory. The power capture for the cases where the device operates at resonance either by optimal reactive phase control or by the choice of incident wave period (T=10.25s) is significantly greater than that for the device operating without phase control. However, the predicted amplitudes of motion for real-world deployment of WECs are unrealistic. In addition to optimal phase control, the results for power absorption via the linear damping PTO mechanism are analysed with sub-optimal phase control whereby the resonance condition is approximately satisfied by latching. These simulations of latching control also lead to large increases in the device response and hence power absorption capabilities of the device. Finally, the results of a simulation of linear and quadratic power take-off for comparison with equivalent linear time-domain results from section 6.4 of WG1 WP1 D3 are also presented and qualitative agreement is observed.

For the array with four devices a less comprehensive set of control strategy/ PTO force combinations is considered than for the single device case given the increase in computational cost associated with simulating a significantly more complex interaction. The action of the nonlinear Coulomb damping PTO force on the devices in the array is simulated and the responses of the devices in the array are compared to those of the single device in isolation. In these comparisons, the single-device PTO force coefficient is used for each of the four devices and the results indicate that the first device to experience the incident waves absorbs more power than the devices behind. Furthermore, each device in the array generally absorbs less power than the single device in isolation. The report concludes with a summary of the results and a general discussion of the main findings in the simulation results and a discussion of lessons learned from the analysis of the results.

1.2 WG1 WP1 D10 acceptance criteria

The acceptance criteria for WG1 WP1 D10 are as follows:

"*Results will be calculated and presented for fully nonlinear responses and power take-off from controlled axisymmetric devices in regular waves. Devices in isolation and in square arrays of four units will be assessed. Linear and nonlinear PTOs will be assessed along with different control strategies. In so far as it is possible prior to validation, findings will be discussed and applications and limitations of this approach will be described, including any lessons-learned on methodology*."

The sections addressing these criteria are sections 3 and 4 containing, respectively, the fully nonlinear responses for the controlled single device and devices in a square array of four units in regular waves subject to linear and nonlinear PTOs under different control strategies. Each section contains some analysis of the response and power take-off and some cross-comparisons with linear theory are also made.

2 BASIC WEC CONTROL AND PTO THEORY

Before describing the various control strategies and PTO forces that have been simulated it is useful to summarise the basic WEC control theory described in section 3.6.2 of the methodology report WG1 WP1 D1B. Although the OXPOT simulations model the fully nonlinear hydrodynamics involved in the interaction of the device and surrounding fluid, the linear theory from the aforementioned deliverable provides a good basis for the description on the device control and power take-off. Furthermore, for weakly nonlinear interactions, the linear component of the motions will dominate so it is expected that many of the results from linear theory will be broadly applicable to the fully nonlinear simulations.

2.1 Equation of motion of the body and the effect of PTO forces

The equation of motion for a device of mass M and waterplane area W constrained to move in heave is given by

$$M\ddot{x}_3(t) = -\rho \iint_\Gamma \frac{\partial \Phi}{\partial t} n_3 dS - \rho g W x_3(t) + F_{PTO}(t) + F_{CON}(t), \quad (1)$$

where ρ and g are the density of the water and acceleration due to gravity, x_3 is the heave displacement, $F_{PTO}(t)$ and $F_{CON}(t)$ is the force exerted on the device by the PTO and control mechanisms, respectively, and Φ is the velocity potential. The vertical component of the hydrodynamic pressure force (pressure given by $p = -\partial\Phi/\partial t$) is integrated over the surface Γ of the device to give the total wave force on the body. If Φ must satisfy the fully nonlinear water-wave equations then it is difficult to decompose the total hydrodynamic force into separate components due to wave excitation, body motion etc. Therefore, before attempting to analyse the fully nonlinear response of the body subject to (possibly) nonlinear PTO forces and control methods it is useful to adopt the standard linearising assumptions and analyse this simplified model. In the linear theory the potential can be decomposed as

$$\Phi = \Phi_I + \Phi_D + \Phi_R \quad (2)$$

where Φ_I is the incident wave potential, Φ_D the diffracted wave potential and Φ_R the radiation potential. The incident and diffracted potential are generally considered together (sometimes referred to as the scattering potential) with the exciting force due to the diffraction of the incident wave being defined as

$$F_{EX}(t) = -\rho \iint_\Gamma \frac{\partial}{\partial t} (\Phi_I + \Phi_D) n_3 \, dS. \quad (3)$$

The radiation potential Φ_R describes the wave field due to oscillations of the body in the heave mode with a velocity amplitude $v_3(t)$ and the associated radiation force is

$$F_{RAD}(t) = -\rho \iint_\Gamma \frac{\partial \Phi_R}{\partial t} \, n_3 \, dS \quad (4)$$

If the PTO and control mechanism is modelled as a linear spring-damper system then the force exerted on the device is given by

$$F_{PTO}(t) = -\gamma_{33} \, \dot{x}_3(t) - k_{33} x_3(t) \quad (5)$$

where the first term models the power take-off and the second term models the control. The double subscripts on the damping and spring coefficients (γ and k) are present because, for fully unconstrained motions, it is possible to have damping and restoring forces in all modes of motion and coupling between modes is also possible. Substituting for the radiation, excitation and PTO forces, the linearised time-domain equation of motion of the device can be written as

$$M\ddot{x}_3(t) + \gamma_{33}\dot{x}_3(t) + (k_{33} + \rho g W)x_3(t) - F_{RAD}(t) = F_{EX}(t) \quad (6)$$

where the radiation force has been brought to the left hand side because of its dependence on the body velocity. This equation is coupled to governing equations of the wave motion through the boundary condition for the normal fluid flow at the device and the presence of the velocity potential in the radiation and excitation forces above. Even in the linearised theory the time-domain problem is very difficult to solve and to understand the basic WEC theory it is necessary to assume the motion of the waves and body are regular (with a time dependence $e^{-i\omega t}$) and to consider the problem in the frequency-domain. Therefore, the displacement and velocity of the body are written $x_3(t) = Re(\xi_3(\omega)e^{-i\omega t})$ and $v_3(t) = Re\left(u_3(\omega)e^{-i\omega t}\right)$, respectively, and the velocity potentials as $\Phi = Re(\phi e^{-i\omega t})$. Typically, the radiation potential is expressed as the product of the velocity amplitude and the velocity potential ϕ_3, i.e.

$$\Phi_R = Re\left(u_3\phi_3 e^{-i\omega t}\right), \quad (7)$$

so that ϕ_3 describes the wave motion of the fluid due to the motion of the body in heave with unit velocity amplitude. The expression of the radiation potential in this form allows the total radiation force to be decomposed as

$$F_{RAD}(t) = u_3(\omega)(i\omega(a_{33}(\omega) + ib_{33}(\omega)/\omega) \quad (8)$$

where a_{33} and b_{33} are the added mass and damping coefficients (for heave motions only) which are in phase with device acceleration and velocity respectively. By writing the radiation force in this way, the equation of motion for the device can be solved in terms of the velocity amplitude as follows

$$u_3(\omega) = \frac{i\omega X_3(\omega)}{\omega^2(M + a_{33}) - (\rho g\, W + k_{33}) + i\omega(\gamma_{33} + b_{33})} \quad (9)$$

where $X_3(\omega)$ is the exciting force amplitude in heave.

The instantaneous power absorbed through the linear damping PTO mechanism is simply the product of the PTO force and the velocity i.e.

$$P_{ABS}(t) = F_{PTO}(t)\dot{x}_3(t) = \gamma_{33}\dot{x}_3^2 + k_{33}x_3\dot{x}_3 \quad (10)$$

The power absorbed through the damping force is of most interest; the restoring force term is sometimes referred to as reactive power and in regular waves over a single period it has a mean value of zero. It is straightforward to investigate the effect of the strength of the damping coefficient on both the motion of the body, by comparing $(x_3(t), \dot{x}_3(t))$ for each case, and also the total power absorbed. Therefore, a number of simulations involving different linear PTO coefficients γ are

conducted. A nonlinear PTO mechanism is also modelled based on the PTO to be utilised in the QUB experimental investigations. In a fully nonlinear description of the hydrodynamic response of a body to regular incident waves the inclusion of nonlinear terms in the equation of motion of the body poses no problems. By comparing the body responses and power absorption profile for each PTO it should be possible to draw some conclusions about the importance of non-linearity in the equations of motion of the devices. Furthermore, in addition to these passive control mechanisms, a brief study of latching will also be conducted for the case of power extracted by a linear PTO.

Some general results from the power absorption theory for linear hydrodynamics are derived next as they will be referred to throughout the report. Firstly, given that the device is constrained to oscillate purely in heave, the subscripts on the dynamic quantities (displacement and velocity) and on the hydrodynamic and PTO coefficients are dropped. The instantaneous power absorbed by the linear PTO is given by

$$P_{ABS}(t) = F_{PTO}(t)\dot{x}(t), \tag{11}$$

and the corresponding mean power over a single wave period in regular waves is

$$P_M = \frac{1}{4}(\hat{F}_P u^* + \hat{F}_P^* u) \tag{12}$$

where $\hat{F}$ and u are the complex force and velocity amplitudes in regular waves with a time dependence $e^{-i\omega t}$. If the power take-off force is modelled as a linear damper and restoring force then the mean power is given by

$$P_M = \frac{1}{2}\gamma|u|^2 \tag{13}$$

because the mean contribution of the restoring force term is zero over a single period. The velocity of the device undergoing excitation from an incident wave subject to the linear PTO and control forces (modelled as a linear spring and damper) has already been solved for and so the mean power absorbed can be re-expressed as

$$P_M = \frac{\gamma\omega^2|X|^2/2}{\{\omega^2(M+a) - (\rho g W + k)\}^2 + \omega^2(\gamma + b)}. \tag{14}$$

Falnes (2002) discusses how this power can be maximised by first assuming the mass and 'stiffness' or reactance of the system is fixed and varying the damping coefficient γ in order to determine γ_{opt} . The maximised linear damping coefficient and power absorbed at this maximal state are

$$\gamma = \left\{ b^2 + \left(\omega(m+a) - \frac{(\rho g\, W + k)}{\omega} \right)^2 \right\}^{1/2} \tag{15}$$

and

$$P_M = \frac{|X|^2/4}{b + \left\{ b^2 + \left(\omega(m+a) - \frac{(\rho g\, W + k)}{\omega} \right)^2 \right\}^{1/2}}. \tag{16}$$

and this can be further optimised if we assume the spring stiffness k can be tuned to achieve the resonance condition

$$\omega^2(m+a) - \rho g W + k = 0 \tag{17}$$

so that the optimal power is

$$P_M = \frac{|X|^2}{8b}. \tag{18}$$

The optimal damping coefficient and velocity are given by

$$\gamma = b \tag{19}$$

and

$$u = \frac{X}{2b}. \tag{20}$$

The resonance condition ensures the velocity of the device is in phase with the exciting force because the imaginary term in (9) vanishes and is sometimes referred to as the optimum phase condition. The optimum phase condition holds irrespective of the value of the linear damping coefficient – equation (15) is referred to as the optimum amplitude and when the conditions are satisfied simultaneously then the damping coefficient satisfies (19) and the power absorbed attains its optimal value (18). The optimal phase condition is of particular importance because, as we will discuss later, it is possible to ensure the velocity and exciting force are in phase using discrete and continuous control mechanisms. It should be emphasised that these results have been derived in the linearised frequency-domain framework and thus are only valid for small regular, monochromatic waves.

The previous optimum power absorbed expressions can also be obtained by neglecting the dynamics of the system (i.e. allowing the velocity to be freely selected rather than constrained by the equation of motion) and attempting to optimise the power absorbed in terms of the velocity. (Thomas & Evans, 1981) adopted this approach for a multiple bodies moving only in heave. The mean power absorbed is computed by taking the time average of the product of the total force and device velocity vectors generalised for an array of multiple devices. The maximum power absorbed is achieved by choosing the velocity vector $\boldsymbol{U}$ to satisfy

$$\boldsymbol{U} = \frac{1}{2}\boldsymbol{B}^{-1}\boldsymbol{X} \tag{21}$$

where $\boldsymbol{B}$ is the generalised damping coefficient matrix, $\boldsymbol{X}$ is the exciting force vector where the n^{th} element of $\boldsymbol{X}$ and $\boldsymbol{U}$ are the exciting force on and velocity of the n^{th} device. The corresponding maximum power is

$$P_M = \frac{1}{8}\boldsymbol{X}^*\boldsymbol{B}^{-1}\boldsymbol{X}. \tag{22}$$

No mooring or power take-off forces are considered in this approach; however, to realise the optimal device amplitudes some degree of control of the devices may be necessary. Clearly, for the special case of a single device these results agree with (11) and (9) respectively for the case where the power is optimised in terms of the power take-off subject to the equation of motion of the body. Therefore, a linear spring-damper control/PTO system is one method for realising optimum device velocity amplitudes.

2.2 Control strategies

The implementation of control strategies is generally dependent on the details of the PTO mechanism. However, in the idealised model of PTO described above for a device in regular incident waves it is nevertheless possible to discuss a number of different available strategies in order to maximise the power extracted. The details of how these control strategies are implemented will not be discussed – the effect of the control on the dynamics of the system and the power absorbed is of primary interest.

Maximum power take-off in regular waves is achieved by satisfying both the optimum phase (17) and amplitude (15) conditions. Therefore, to achieve optimal power extraction control of the phase and amplitude of the device motion is necessary. In the time-domain, for regular and irregular waves, the control necessary to achieve maximum power take-off is referred to as continuous optimal control or reactive control. In linear regular waves, the optimal conditions can be satisfied by choice of the linear spring and damping coefficients whereas in irregular waves some future knowledge of the incident wave is required in order to satisfy the phase condition in particular. In all cases it is necessary to adjust the power take-off damping to achieve the optimal motion amplitude – in regular waves the PTO damping is a constant whereas in irregular waves it may vary continuously in time. In order to achieve the required phase control a number of different strategies can be implemented.

Phase control can fall into two categories – continuous (or reactive) phase control and discrete control. In the former, the controller can act on the device at any instant during the power absorption cycle in order to adjust the so-called reactance of the oscillating system (see (Falnes, 2002) for details). This may involve controlling the reactive power of the system to maximise the active power, i.e. a reversal of the energy through the PTO system may occur during parts of the absorption cycle meaning energy will be delivered back into the surrounding fluid. In the latter, the controller acts on the device only at a finite number of instants during the cycle. Latching is an example of discrete control suggested by (Budal & Falnes, 1980) among others for point absorbers with natural periods of oscillations shorter than the incident waves. Latching approximately satisfies the optimal phase condition by locking the device in place at the extremity of the motions (zero velocity) and releasing at the instant when the excitation force is back in phase with the velocity. Thus, the natural oscillation is effectively slowed down to match that of the incident wave. The interval over which the device is latched is pre-determined and is known as the latching duration – it is the only variable to be determined in the control problem. The subject of latching control has been widely investigated in recent times; (Clement & Babarit, 2012) provide an excellent description of the method and discuss and present results for a device in regular waves in the context of other discrete control methods (e.g. declutching).

Although discrete latching control only approximately satisfies the phase conditions it is nevertheless observed to yield significant gains in the power absorbed from an incident wave compared to an uncontrolled device or a controlled device which doesn't satisfy the phase condition. In the following investigations the power absorption performance of a device operating with a constant linear spring coefficient and with latching control will be compared for the cases where the incident wave frequency are lower than the natural frequency of the device. Latching control can also be implemented for incident wave frequencies higher than natural frequency of the device; however, it is more straightforward to consider the aforementioned case.

It should be noted that the OXPOT simulations involving power take-off and control of the wave energy device (modelled as a truncated cylinder) involve fully nonlinear hydrodynamics. The preceding linear theory should nevertheless be applicable once the interactions are sufficiently weakly nonlinear. Provided the linear component of the device motion dominates then the results should be very similar to linear frequency domain theory.

2.3 PTO forces

The power will be extracted from the motion of the device through the application of different PTO forces. The first case considered will be the classical linear damping PTO force

$$F_{PTO}(t) = \gamma \dot{x}(t), \tag{23}$$

and the variation in the power absorbed due to changes in the damping coefficient will be investigated. In particular, this damping coefficient will be specified to take values around the optimal value according to the linear theory (19).

A non-linear PTO force will also be considered and the effect of the nonlinearity on the response of the body and the power take-off will be compared to the linear case. The particular non-linear PTO force considered is a Coulomb damping force due to sliding friction. This models the wave energy converter (WEC) brake that will be employed in the QUB experimental investigations to extract energy from the motion of the converter. The magnitude of the sliding friction is independent of the device displacement and velocity; the direction of the force always opposes the motion so that the Coulomb damping friction force can be modelled as

$$F_{PTO-NL}(t) = \begin{cases} -\mu, & for\ \dot{x}(t) > 0 \\ \mu, & for\ \dot{x}(t) < 0 \end{cases}. \tag{24}$$

The value of the constant friction coefficient μ will be chosen so that the force over a cycle is comparable to the RMS value of the linear damping force i.e. $\mu = \gamma\, u/\sqrt{2}$, where u is the velocity amplitude for the linear problem.

3 SINGLE CONTROLLED DEVICE IN REGULAR SEAS

3.1 Case studies

Three interactions involving a single truncated cylinder will be considered. The particular truncated cylinder considered is the same as that specified in table 4 of WG1 WP1 D9. For ease of reference it is reproduced here in Table 1. The three interactions involve incident waves of period $9s$, $10.25s$ and 15s with amplitudes of $2m$, $3m$ and $2m$ corresponding to waves of higher frequency than the natural response frequency, equal to the natural frequency and lower than the natural response frequency, respectively. The latter incident wave is investigated to allow the effects of latching control to be investigated in a straightforward way.

Property	SI unit	Dimensionless value
Water depth	$80m$	1.0
Cylinder Diameter	$20m$	0.25
Cylinder Draft	$20m$	0.25
Volume of displaced water	$6.28 \times 10^3\ m^3$	1.227×10^{-2}
Cylinder Mass	$6.44 \times 10^6\ kg$	1.227×10^{-2}
Position of centre of mass (x_{CM}, y_{CM}, z_{CM})	$(0.0,0.0,-14.59m)$	$(0.0,0.0,-0.182375)$
Inertia matrix (I_{11}, I_{22}, I_{33})	$(2.38, 2.38,1.82) \times 10^8 kgm^2$	$(7.10, 7.10,5.43) \times 10^{-5}$

Table 1: Main geometric properties associated with the cylinder.

At each frequency, different types of power take-off and control will be explored and compared. For example, a power take-off described by a linear damping force will be considered in all cases and compared to the nonlinear Coulomb damping power take-off force. In addition to the different power take-off forces considered, different control mechanisms will be investigated and compared to the uncontrolled operation of the device. For example, the natural frequency of the system will be adjusted by choice of a linear restoring force in order to approach the resonance condition (17) and hence to improve the power absorption capabilities of the system in comparison to the case where the body moves in an uncontrolled manner. In addition to reactive control, discrete phase control will be investigated for the longest wave by using the latching control strategy. In this manner, it should be possible to draw some conclusions regarding the importance of non-linearity on the response of the system. More importantly, it should be possible to examine the effects of different control and power take-off strategies on the performance of a single device in regular waves.

3.2 Power take-off for a cylinder in regular waves of period T=9s and height H=4m

The first simulation corresponded to the truncated cylinder undergoing oscillations in heave in response to a regular wave of incident wave period $T = 9\ s$. Denoting the depth of the fluid domain by h, the numerical wave tank was of total length $7.5\ h$ and width $1.25\ h$ where the wavelength was approximately $1.57h$. Such a domain was used to analyse the uncontrolled response of the truncated cylinder in D9 and more details on the discretisation of the domain are given there. Furthermore, a more detailed description of a typical computational domain for a single cylinder is given in section 3.5. The details of the domain are reproduced here in Table 2 and Figure 1 illustrates the free-surface mesh for this set of OXPOT simulations. The simulations (uncontrolled motion, uncontrolled power take-off, controlled power take-off) were 16-20 periods in duration with time-steps of one-fortieth of a period $(0.025T)$. The effect of the different power take-off and control methods will be examined over the complete duration of the simulation by considering and comparing the power take-off and response time-histories.

Wave (T [s],H [m])	Wavelength λ/h	Amplitude A/h	Length L/h	Width W/h	Number of Elements	Number of Nodes
(9, 4)	1.58	0.025	7.0	1.25	3145	8689
(10,6)	2.05	0.0375	9.0	3.0	3887	10875
(15,4)	4.02	0.025	18.0	4.8	3205	8733

Table 2: Domain and mesh specifications for the numerical wave tanks involved in the wave propagation investigations.

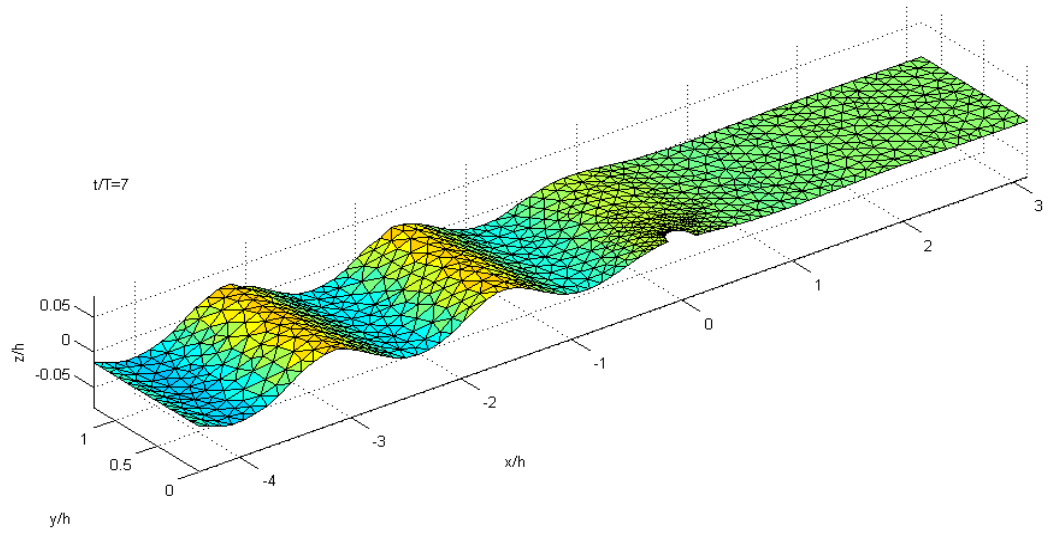

Figure 1: Free-surface mesh for the T=9s, H=4 s incident wave and truncated cylinder interaction.

The optimal power extraction conditions for a linear PTO in regular waves require that both the phase condition (17) and the optimal amplitude condition (15) are satisfied simultaneously; substitution of the former condition into the latter yields the damping coefficient (19) for maximum power extraction assuming the phase condition has been satisfied. In the first set of simulations conducted, the power take-off force consisted purely of a linear damping term so that the spring restoring force term $-k_{PTO}x$ (used to control the phase of the oscillations) was set to zero. Therefore, the optimal damping coefficient in this case is given by equation (15). The frequency domain added mass and damping coefficients are obtained from the results of WG1 WP1 D8 and so the non-dimensional linear damping coefficient is given by

$$\tilde{\gamma} = \gamma_{opt}/(\rho h^3\sqrt{g/h}) \simeq 0.0069. \tag{25}$$

In the case where the phase condition is satisfied, the optimal damping coefficient is

$$\gamma_{OPT} = b. \tag{26}$$

which in non-dimensional terms is $\tilde{\gamma}_{OPT} = 0.00061$. In the following, the power extracted from the regular incident waves is measured first for the uncontrolled motion (k_{PTO}=0) of the device at various values of the linear damping coefficient γ and then with control such that the linear optimal phase condition

$$k_{OPT} = \rho g W - \omega^2(m + a) \tag{27}$$

is satisfied which, in non-dimensional terms, gives $k_{OPT}/(\rho g h^2) = 0.0137$. In all cases the response of the device will be compared to the uncontrolled response over the same period of time.

3.2.1 Linear damping power take-off force

The heave displacement and velocity response of the truncated cylinder to a regular incident wave with a period of 9 seconds for three linear damping PTO coefficients $\gamma = \{0, \gamma_{OPT}/3, \gamma_{OPT}\}$ are shown in Figure 2. It is evident that by increasing the damping force due to the power take-off mechanism the variation in the motion from steady state oscillations due to the transient excitation of the natural resonance of the body is reduced. In particular, it can be observed that the variation in the oscillation amplitude over the course of the simulation is largest for the undamped heave oscillations, whereas for the largest damping coefficient $(\gamma = \gamma_{OPT})$ the device motion has essentially settled into a steady state oscillation. This steady state behaviour can be confirmed by comparing the linear frequency-domain prediction for the motion and power absorption of the optimally damped device to the fully nonlinear OXPOT simulations results as is done in Figure 3. The OXPOT results overestimate the amplitude of the displacement oscillations; however, the phases of the signals agree exactly and the difference in the amplitudes is just 10%. Such a discrepancy can arise from side wall reflections as was observed in WG1 WP1 D9 and also due to non-linear hydrodynamic effects. Nevertheless, in WG1 WP1 D9 the most significant contributor to the difference for weakly nonlinear waves was observed to be the side-wall reflections. In the analysis of the power absorption simulation results, where the response is dominated by the steady state component, the mean power will be considered; but where the response varies significantly over the simulation, the overall trends and variations in the power absorption and displacement time-histories will be considered.

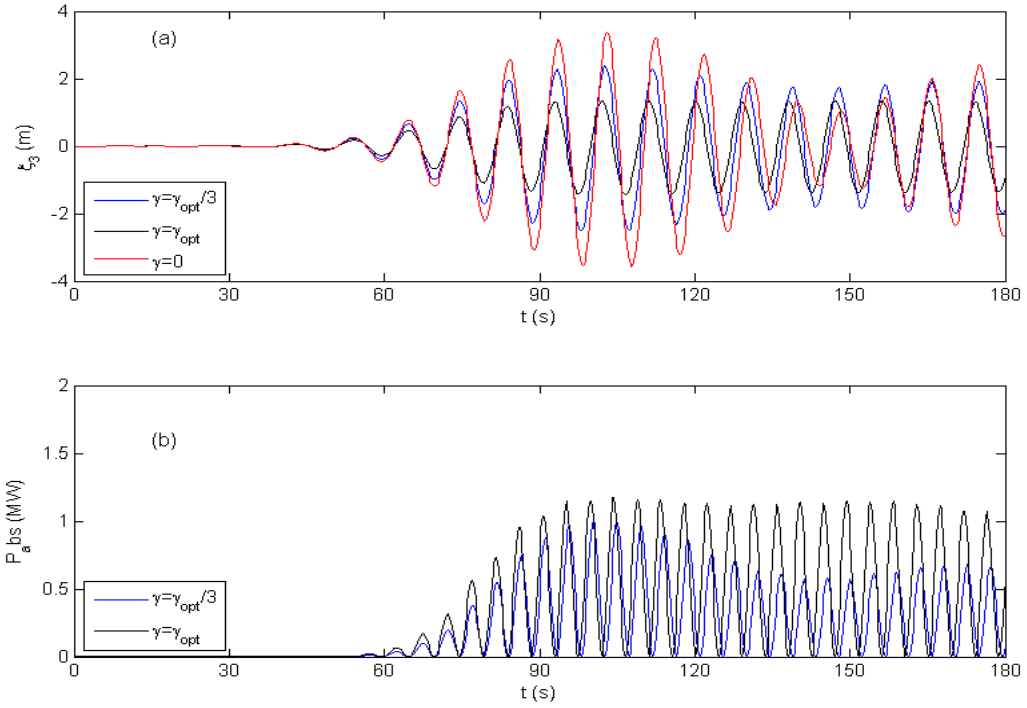

Figure 2: (a) Displacement and (b) power absorbed by a truncated cylinder undergoing excitation from regular incident wave with zero damping (red) and linear damping coefficients $\boldsymbol{\gamma = \gamma_{opt}/3}$ (blue) and $\gamma = \gamma_{opt}$ (black).

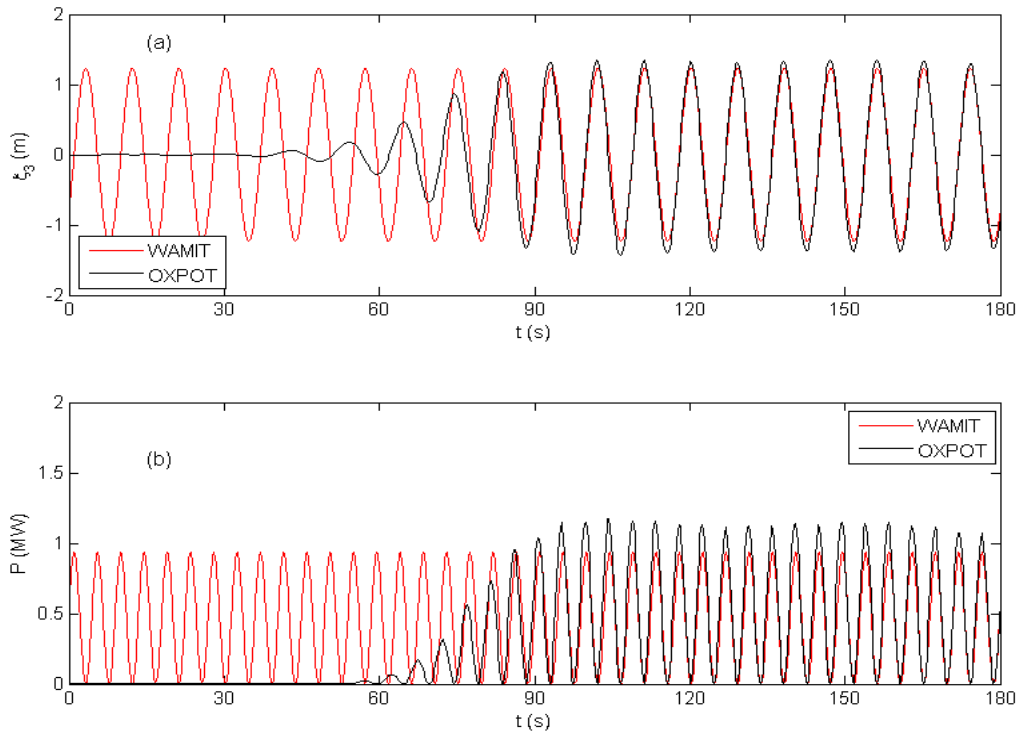

Figure 3: Comparison of WAMIT (red) and OXPOT (black) results for the heave displacement and power absorbed for a device with damping coefficient $\gamma = \gamma_{opt}$ and $k = 0$ in regular waves of period $T = 9s$ and height $H = 4m$.

The importance of phase control on power take-off can be illustrated by changing the so-called reactance of the system so that the resonance condition is satisfied. In the fully nonlinear numerical model of the operation of a heaving point absorber in regular waves this means adjusting the stiffness of the system through a spring restoring force contribution in the PTO/control term. Therefore, the total PTO force acting on the device is $f_{PTO} = -k_{OPT}x(t) - \gamma_{OPT}\dot{x}(t)$ where the spring and damping coefficients are those quoted after conditions (26) and (27) . The resonance condition (17) can be rearranged to give an estimate of the natural frequency of the oscillations

$$\omega_n = \sqrt{\frac{\rho g W + k}{m + a_{33}}} \tag{28}$$

and for the spring coefficient $k = 0$ the natural frequency corresponds to the period $T_n = 10.17s$ whereas for $k_{OPT}/(\rho g h^2) = 0.0137$ the natural period is $T_n = 9.0s$. Therefore, by tuning the response of the device to the waves (through the specification of the value of k) it is possible to achieve resonance. This resonant aspect of the interaction is clearly present in the response of the structure to the incident waves in Figure 4. The comparison with the motion of the structure with a optimal damping but no phase control highlights the increase in the amplitude of the device motion due to the introduction of phase control. Furthermore, the resonant device motion does not settle to a steady state over the first 20 cycles and continues to increase at the end of the simulation. The linear frequency domain theory predicts a steady state motion of $\xi_3 \simeq 10\ m$. In practical terms this will not be achievable, nevertheless in order to optimise power absorption it is clear that phase control plays a crucial role.

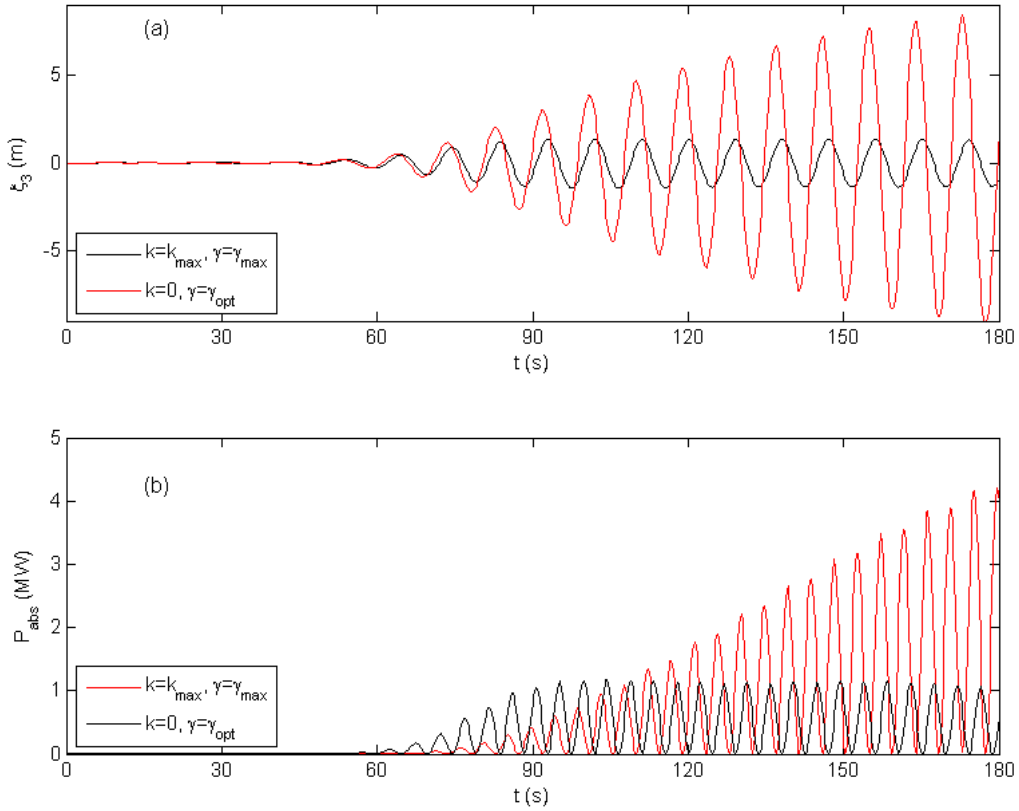

Figure 4: Comparison of (a) displacement and (b) power absorbed by the truncated cylinder in regular waves ($T = 9s, H = 4m$) with no phase control and optimal amplitude control (black) and (b) optimal phase control and optimal amplitude control.

3.2.2 Non-linear power take off force

The effect of the Coulomb damping wave-energy converter PTO mechanism on the dynamics and power extraction capabilities of the single device system was also investigated using the OXPOT numerical simulation method. Of particular interest is how the dynamics of the heaving device with the non-linear power take-off compare to those of an equivalent linear PTO device configuration. Therefore, a number of simulations for different values of μ, the constant force opposing the motion of the device first used in (24), were conducted and are compared to existing linear results next. Choosing a suitable μ value is difficult because it must correspond to the linear oscillating PTO force, which in regular waves, is approximately $\gamma Re[u_3 e^{-i\omega t}]$ where u_3 is the steady state velocity for a given PTO force and stiffness coefficient obtained from (9). To approximate the effect of this force with a non-linear force, the root mean square amplitude of the linear steady state damping force was used so that $\mu = \gamma u_3/\sqrt{2} = \mu_0$.

In order to approximate the linear PTO force due the damping coefficient $\gamma = \gamma_{opt}/3$ ($0.37Nsm^{-1}$ in SI units) a Coulomb damping force of $\mu = 0.28MN$ was used. No phase control was implemented in either simulation ($k = 0$). The results of the two simulations are compared in Figure 5. The displacement time-histories are quite similar although the displacement of the device with Coulomb damping has a larger maximum around the time $t \simeq 100$ at which point the linear damping force has signficantly larger extrema than the Coulomb damping force (see Figure 5 (c)). This figure

containing the power take-off force time histories shows the fundamental difference between the linear damper and the Coulomb damper, namely that the linear damping force has sharp peaks at maximum velocity whereas the Coulomb damping remains constant throughout the motion in a given direction. Consequently, the power extracted by the Coulomb damper (also referred to as the WEC brake) has significantly smaller peaks than the linear damper. Integration of the power absorbed signals reveals that mean power extracted over the duration of the simulation by the linear damping and nonlinear PTO force is approximately $0.37\ MW$ and $0.25\ MW$, respectively, that is the power extraction by the linear PTO is 50% greater than for the nonlinear PTO *for a similar device response*.

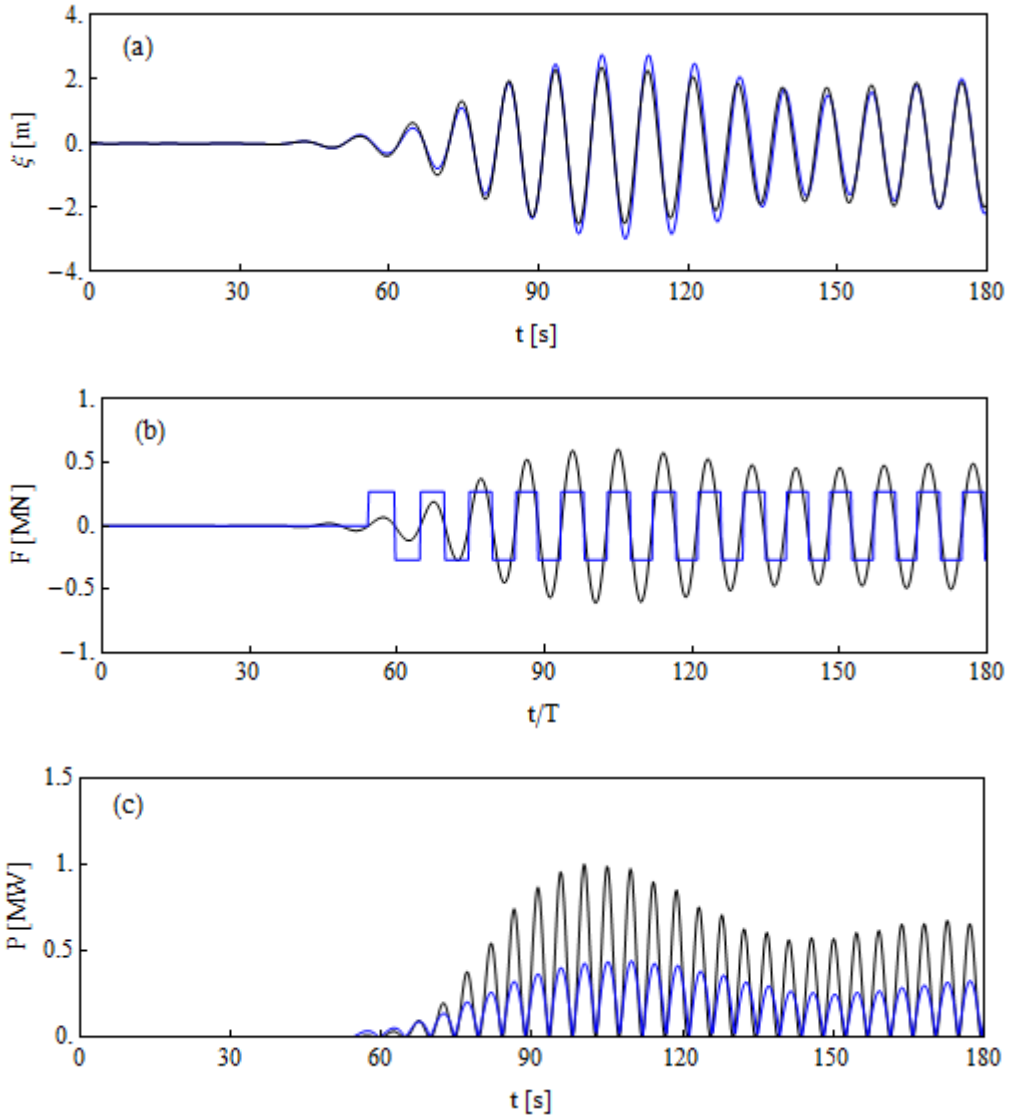

Figure 5: (a) Device displacement, (b) device PTO force and (c) power extracted from waves for the linear PTO damping force with coefficient $\gamma = 0.37\ MNsm^{-1}$ and for the non-linear PTO damping force where $\mu = 0.28\ MN$.

In order to implement the Coulomb damping correctly, it was necessary to allow the motion of the body (and the exciting force exerted on the body) to reach sufficiently large amplitude so that the friction force was less than the dynamic force. Otherwise, the friction force would force the motion of the structure and not dissipate energy from the motion as required. The Coulomb damping force is essentially a sliding friction force and hence there should be no motion of the body when the exciting force amplitude is less than the friction force. Once the exciting force overcomes the friction force then the body can move and the Coulomb damping will act to dissipate energy. In the OXPOT implementation, the Coulomb damping is only applied only after a sufficient number of periods of the simulation have elapsed for the incident wave to have excited a significant motion of the device. In the above simulations, this time was specified to be $t = 6\,T \simeq 54$s. Notice that the amplitude of the corresponding linear damping force approximately equals the constant Coulomb damping force at this time in Figure 5 (b). To achieve a more realistic model of the motion, it may be necessary to measure the exciting force and implement the Coulomb damping once the exciting force amplitude is larger than that of the friction force.

By increasing the Coulomb damping force to $\mu = 0.37MN$ it was expected that the transient motion might be suppressed in a similar manner to the increases in the linear PTO coefficient. Furthermore, it was expected that the mean power absorbed over the simulation should also be larger. The displacement, PTO force and power extracted for the nonlinear PTO are compared to the corresponding quantities for the linear PTO in Figure 6. The dynamics of the response of the device with the nonlinear PTO become progressively more similar to the linear case as the simulation progresses – initially, the larger dissipating force exerted by the nonlinear PTO reduces the amplitude of the device oscillations compared to those for the linear PTO. From around $t \simeq 140s$ the difference between the oscillations is quite small. Over the final 100 seconds of the simulation, the device with the linear PTO extracts an average power of $0.37MW$ while the device with the nonlinear PTO extracts $0.335MW$, that is the ratio of energy extracted by the nonlinear relative to the linear power take-off is 0.9. However, if we consider the last 45 seconds (neglecting the initial peak in the response due to resonant excitation) then the average power extracted for linear and nonlinear power take-off is $0.31\ MW$ and $0.30\ MW$, respectively, and the ratio of energy extracted is 0.96. Given that the device response is similar in both cases, this suggests that it may be possible to utilise a linear PTO to approximate a nonlinear PTO. Nevertheless, the profile of the power taken off, shown in Figure 7, differs in both cases with the signal for nonlinear PTO containing wider and smaller peaks compared to the linear signal.

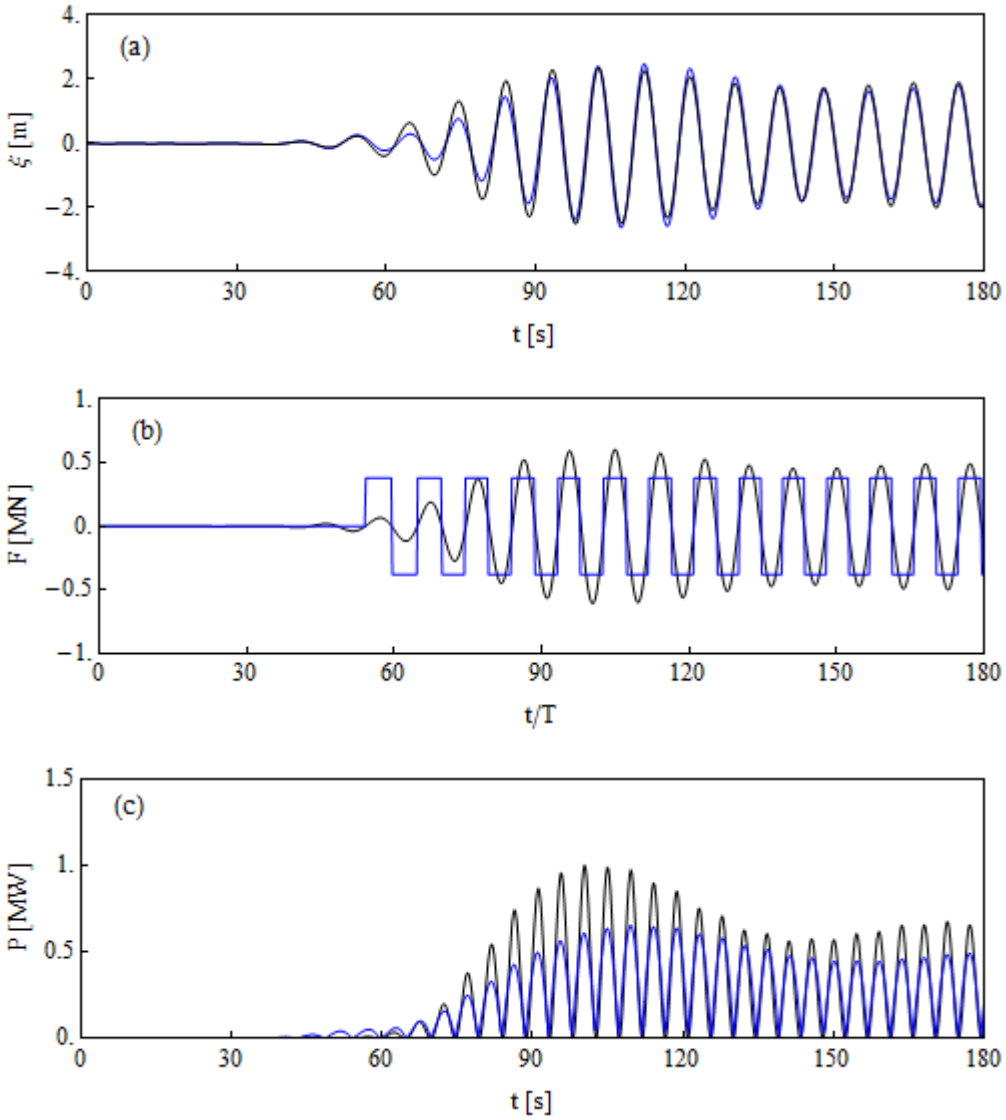

Figure 6: (a) Device displacement, (b) device PTO force and (c) power extracted from waves for the linear PTO (black) with damping coefficient $\gamma = 0.37\ MNsm^{-1}$ (black) and for the non-linear PTO damping force (blue) where $\mu = 0.37\ MN$.

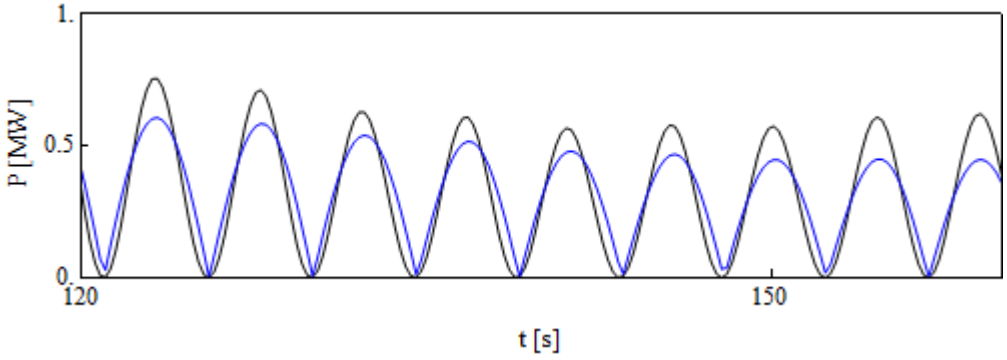

Figure 7: Power absorption signal for the linear (black) and nonlinear (blue) PTO mechanisms.

To emulate the steady-state damped oscillation arising from linear damping with the coefficient $\gamma = \gamma_{opt} = 1.26MNs/m$, a Coulomb damping force constant $\mu = \gamma_{opt}u_{opt}/\sqrt{2}$ (where u_{opt} is the steady state velocity amplitude) was specified. The results are shown in Figure 8. In absolute terms, this Coulomb damping force is $1.09MN$. This force is substantially larger than the previous nonlinear damping forces and thus the effect of nonlinearity on the motion is expected to more significant. The force is not applied until 7.5 periods into the simulation which means the device moves freely as the long, small amplitude waves arrive at the device from the wavemaker. Such motion could be avoided by applying the nonlinear Coulomb damping force once the device displacement amplitude begins to move appreciably. This approach is taken in the simulations of incident waves of longer period (15 seconds) which follow in later subsections. Nevertheless, it is clear from Figure 8 that the behaviour of the device subject to the nonlinear Coulomb damping force is quite similar to that of the device subject to the linear damping force. The displacement amplitudes are slightly larger in the nonlinear case while the amplitude of the power absorption oscillations is greater for the linear PTO force which is as expected. In terms of the average power capture, the device with linear PTO damping extracts $0.55MW$ while the device with nonlinear power take-off extracts $0.53\ MW$ on average over the last 45 seconds of the simulation. Frequency-domain analysis indicates the mean power extracted is approximately $0.47MW$ and the overestimate in the linear case is mostly attributed to the side wall reflections which return diffracted/radiated energy to the device. The results for the set of power take-off simulations with incident waves of period 9 seconds are summarised in Table 3. The final entry in the table is for the absorption of power at resonance and hence the average power capture is significantly larger than in the other cases.

	PTO damping force		**PTO Stiffness**	**Average Power**
PTO, phase control	$\gamma\ (MNs/m)$	$\mu\ (MN)$	$k\ (MN/m)$	$P_M(MW)$
Linear, none	0.37	–	0	0.31
Nonlinear, none	–	0.28	0	0.21
Nonlinear, none	–	0.37	0	0.30
Linear, none	1.26	–	0	0.55
Nonlinear, none	1.09	–	0	0.47
Linear, reactive	0.11	–	0.878	1.72

Table 3: Summary of the average power capture for the simulations of power take-off for regular incident waves of period T=9.0s.

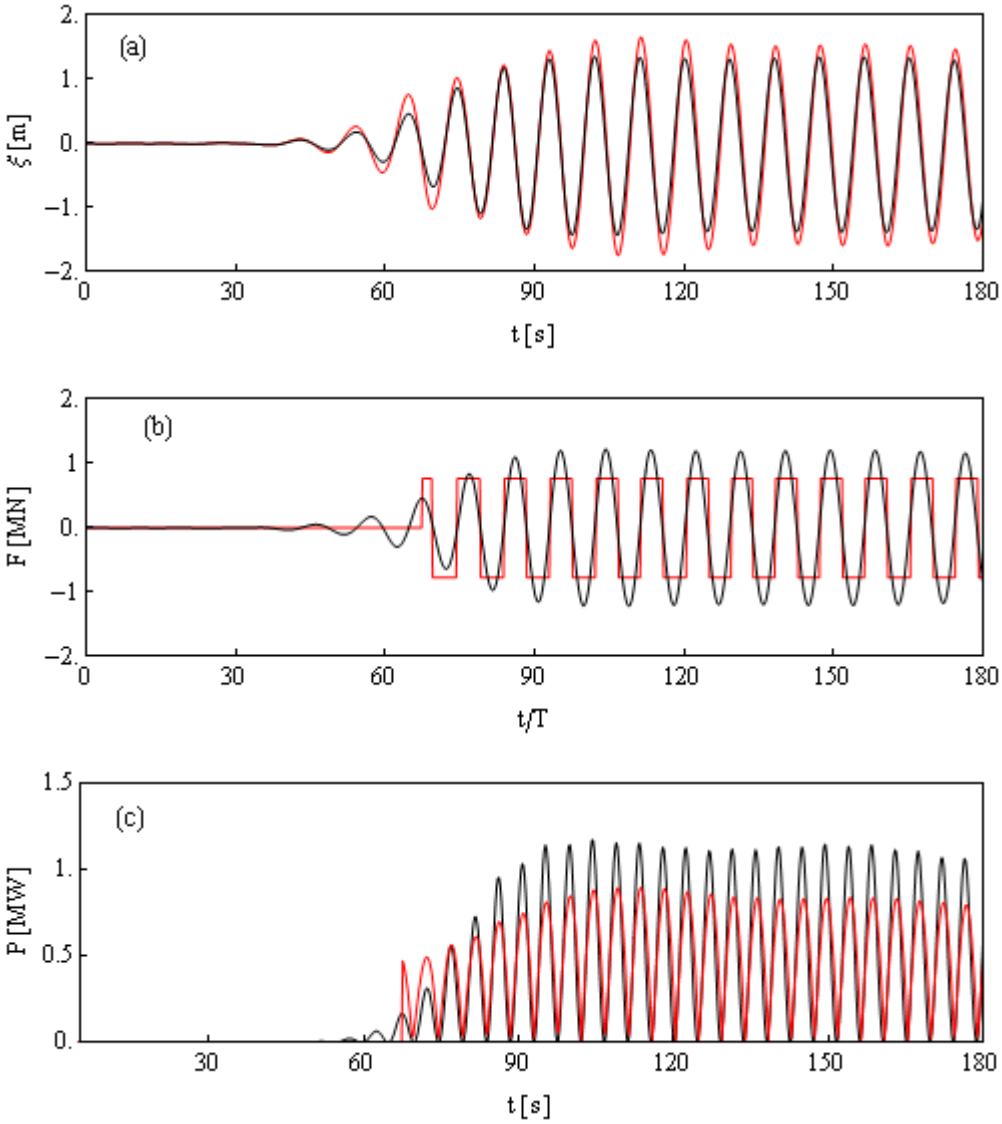

Figure 8: (a) Device displacement, (b) device PTO force and (c) power extracted from waves for the linear PTO (black) with damping coefficient $\gamma = 1.26\ MNsm^{-1}$ (black) and for the non-linear PTO damping force (red) where $\mu = 1.09\ MN$.

3.3 Power take-off for a cylinder in regular waves of period T=10.25s and height H=6m

It has been observed previously (WG1 WP1 D8, WG1 WP1 D9) that the truncated cylinder has a natural (heave) resonance at the period $T \simeq 10.25\ s$ approximately. Therefore, in incident waves of the same period the motion of the device will build-up towards a large steady-state oscillation from an initial state of rest just as the device with optimal control in Figure 4 (a). However, the device in this case operates at resonance in incident waves of period 10.25 seconds and hence no phase control is necessary – the optimal phase condition (17) is already satisfied and so the exciting force and device velocity are in phase. Therefore, to achieve maximum power absorption the linear damping coefficient must equal the heave radiation damping coefficient, i.e. equation (19) must be satisfied.

The optimal damping coefficient can be determined from the frequency domain coefficients as computed in WG1 WP1 D8 using WAMIT. Substituting the added mass and radiation damping coefficients (along with the waterplane area and mass of the device) into the resonance/phase condition (17) reveals that the device is not operating exactly at resonance in waves of period 10.25 seconds – the so-called reactance term $k_{opt} = \rho g W - \omega^2(m + a)$ does not exactly equal zero. In non-dimensional terms, k_{opt} takes the value $0.000562\rho g h^2$ which is two orders of magnitude smaller than the equivalent term for incident waves of period 9 seconds. Therefore, the device operates at a frequency *close to* resonance but the velocity and exciting force are slightly out of phase. The optimal damping coefficient (15) is computed to be

$$\{b^2 + (\omega(m + a) - \rho g\, W/\omega)^2\}^{1/2}/(\rho h^3\sqrt{g/h}) = 0.000837 \tag{29}$$

whereas the damping coefficient at resonance (19) is

$$b/(\rho h^3\sqrt{g/h}) = 0.000774. \tag{30}$$

Clearly, the effect of the reactance term is relatively small and the latter damping coefficient is chosen for the investigation into power absorption by the device operating at near resonance. The damping force acting on the device reduces the amplitude of the oscillations compared to the undamped oscillations as shown in Figure 9 (a). In fact, the OXPOT simulation of the undamped oscillations fails after 15 periods while the numerical solution of the damped resonant motion does not break down until 18 periods have elapsed. The failure of the OXPOT simulation is due to the extremely large oscillations of the cylinder. Referring to Figure 9 (a), it can be seen that cylinder displacement is approaching 20m in the last time steps before the simulation fails. This corresponds to the cylinder 'leaping from the water' or breaking the free-surface completely because the draft of the device is 20m. Given that such displacement amplitudes are impractical in the context of the full scale operation of wave energy devices it is not significant that simulations crash for this case. According to the linear frequency domain theory, the displacement of the undamped motion has an amplitude of 35m and the damped oscillations of 18.5m. The motion of the body with linear PTO almost arrives at steady state (the growth of the displacement oscillations slows towards the end of the simulation) although this steady state will not correspond exactly to the linear steady state due to the nonlinearity in the OXPOT hydrodynamic model. The power extracted through the linear PTO mechanism is significantly larger than for the optimal absorption in incident waves of 9 second period (both with and without phase control, see Figure 4 (b)) and this can be attributed to the larger incident wave height and device operation at resonance. Given that device never settles to the steady state in the case of the linear PTO it is difficult to choose a Coulomb damping force to compare to the linear damping force.

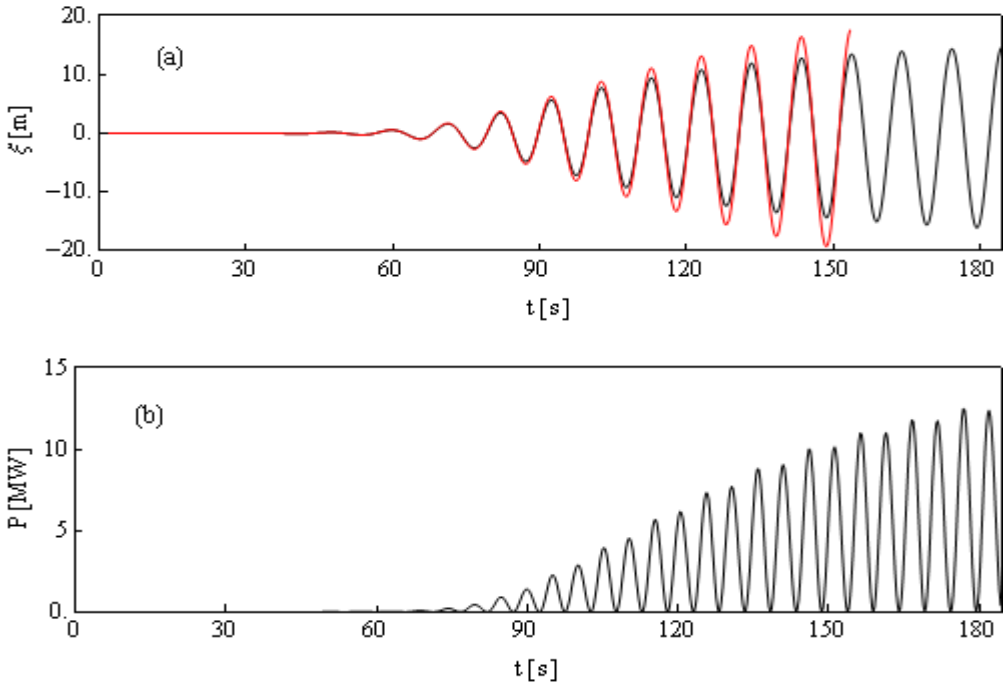

Figure 9: (a) Displacement of device in waves of period 10.25s and height 6m with linear PTO (30) (black) and uncontrolled (red) and (b) power extracted by the linear PTO.

3.4 Power take-off for a cylinder in waves of period T=15.0s and height H=4m

Simulations of the effect of power take-off and control on the dynamics of the truncated cylinder were also conducted for regular incident waves of a longer period (15 seconds) than the natural resonant period of the device (approximately 10.25 seconds). In this case the incident wave period is significantly longer than the natural resonant period of the device and this has a number of advantages for investigating the dynamics of the floating device. Firstly, such a configuration allows the effects of latching control on the motion of the device to be investigated in a relatively straightforward manner because latching control was first introduced as a method of effectively slowing the natural resonant period of the wave energy device to approximately satisfy the phase condition. A brief investigation of latching control will be carried out in addition to the assessments of the different power take-off mechanisms acting on the device. Secondly, the excitation of the transient natural resonant oscillations by incident waves is more significant the closer the incident wave frequency is to the resonant frequency. Therefore, for an incident wave frequency much larger or smaller than the resonant period, the effects of transient motions should be negligible and thus the motion will effectively settle to steady state once the initial wave front has passed. This makes comparisons with linear frequency domain theory much more straightforward.

The details of the half-domain mesh for this incident wave are provided in Table 2 and an illustration of the free-surface mesh is provided in Figure 10. It is clear that the dimensions of the cylinder (radius 10m) are much smaller than that of the incident wavelength (approximately 320m) so that any diffraction effects are small relative to the incident wave. Furthermore, the nonlinearity coefficient $\varepsilon = H/\lambda$ is quite small with a value of 0.0125 – this ensures the comparisons with linear theory can be obtained without recourse to the phase manipulation method described in WG1 WP1 D9 which requires two simulations per interaction.

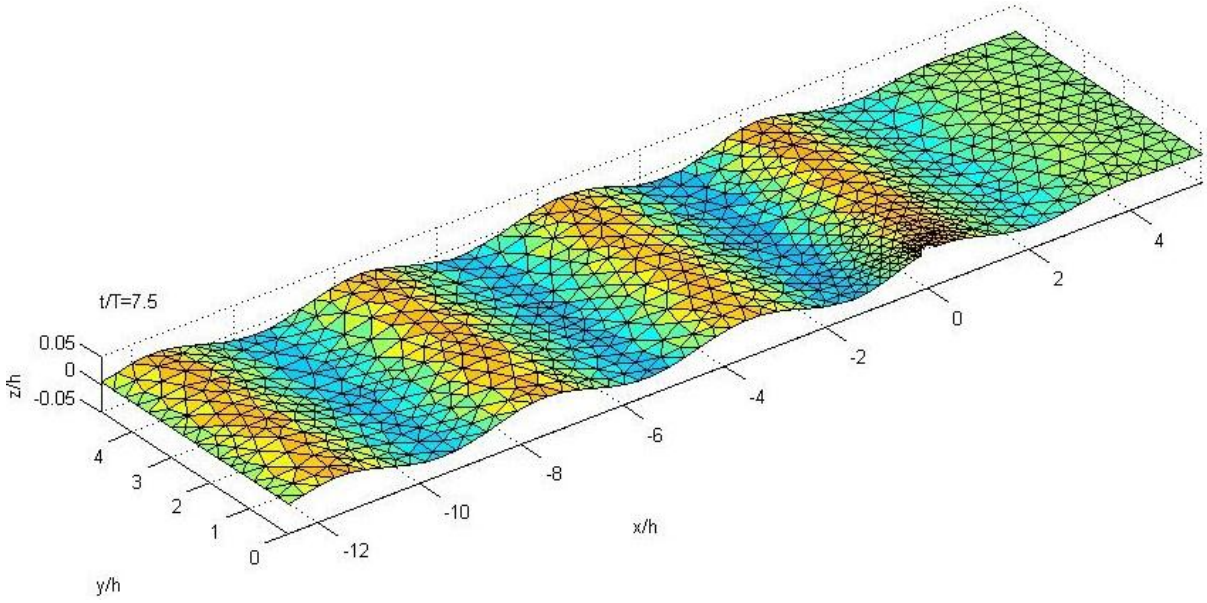

Figure 10: Free-surface mesh for the T=15s, H=4 s incident wave and truncated cylinder interaction

To understand the basic dynamics involved in the operation of the device in such long wave conditions it is useful to first consider the uncontrolled motion of the device before proceeding to the controlled and damped motions (this incident wave was not considered in WG1 WP1 D9). The duration of the uncontrolled motion simulations is sixteen periods (240 seconds) and results for two variations on the basic wave form are presented. In all simulations, the piston wavemaker motion is ramped from rest to purely sinusoidal oscillations using a ramping function

$$f(t) = \frac{1}{2}\left(1 - \cos\frac{\pi t}{t_m}\right), \qquad 0 \le t < t_m \tag{31}$$

to modulate the underlying sinusoidal signal. In the first simulation, the ramping function is employed over the first two wave periods ($t_m = 2T$) and in the second over four wave periods ($t_m = 4T$). Although the device displacement rather than velocity have been presented thus far when illustrating the effects of the transient, here the effects of the transient resonant excitation are clearer in the velocity time-history and so the device velocity for the two incident waves generated by a wavemaker motion with two different ramping periods are shown in Figure 11 where they are compared with the linear frequency domain results. Clearly, the longer the duration over which the wavemaker motion is ramped from rest to full sinusoidal motion, the less resonant excitation occurs. This is because the spectrum of the incident wave generated by a relatively sudden start-up of the wavemaker contains a broader range of frequencies whereas a slow build-up of the wavemaker generates an incident wave with a very narrow spectral peak. If the spectral peak is very narrow then there is much less significant excitation of a natural resonance away from this peak. In the context of the power take-off simulations, the agreement observed between the OXPOT simulation results and linear frequency domain results in Figure 11(b) for the uncontrolled motion can also be expected for motions involving damping by a linear PTO.

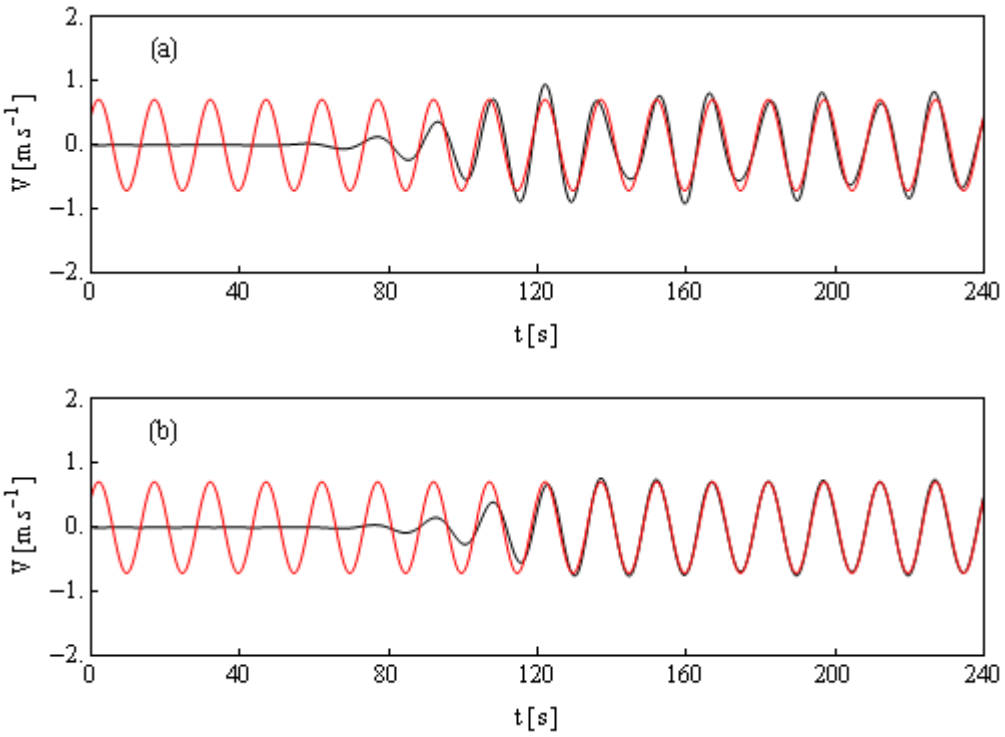

Figure 11: Velocity of the uncontrolled device in regular waves of period 15s generated from wavemaker motions with a ramping duration of (a) two wave periods and (b) four wave periods.

The optimal linear damping coefficient for the truncated cylinder responding to incident waves of period 15 seconds without phase control is calculated from equation (15) to have a non-dimensional value $\tilde{\gamma} = 0.0217$ ($3.99MNs/m$ in SI units). Implementing this linear PTO damping force in OXPOT allows direct comparisons with the frequency domain results for device motion and power absorption. The simulations for the 15 second period waves were run for 16 periods and the comparisons between linear frequency-domain (WAMIT) and fully nonlinear time-domain (OXPOT) are shown in Figure 12. The OXPOT velocity time-history agrees very well with the linear frequency domain prediction; however, there are some (small) discrepancies visible between the OXPOT and WAMIT predictions for the power absorbed. These discrepancies are much more obvious for the power absorbed because it involves the velocity squared and hence any errors in the velocity are magnified when the power extracted is computed. The average power absorbed as computed by OXPOT over the final 6 periods of the simulation is $1.00MW$ which compares favourably with the linear mean power absorbed prediction $0.947MW$ computed from (16). The error is approximately 5.6% and implies an error of 2.3% in the velocity results.

To determine the Coulomb damping PTO force constant μ comparable in magnitude to the linear damping force, the root mean square of the amplitude linear damping force ($\mu = \gamma_{opt} u_{opt}/\sqrt{2}$) was again computed giving a value of $1.94MN$ or $\mu = 0.000378$ in non-dimensional terms. Once again, the frequency domain quantities were used to compute γ_{opt} and the corresponding u_{opt} from equations (15) and (9). In the simulation, the Coulomb damping force is applied after the six periods have elapsed (i.e. after 90 seconds). Some interesting behaviour can be observed in the dynamics of the motion of the body which is compared to the motion for the linear PTO force in Figure 13.

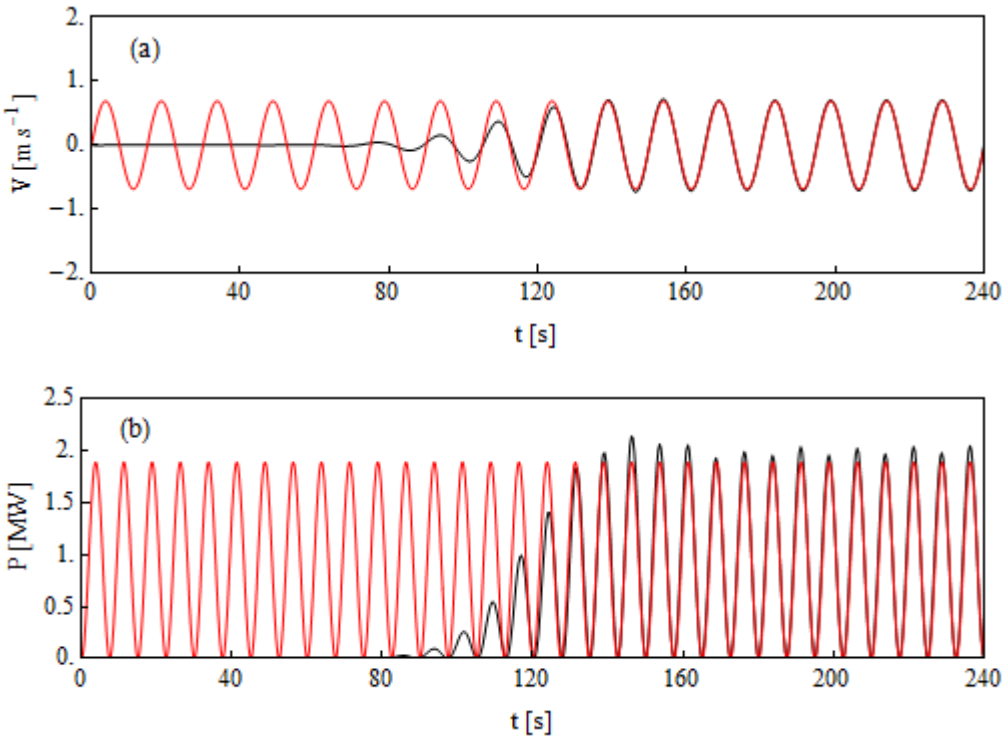

Figure 12: Results for (a) the device velocity and (b) power extracted by the linear PTO for optimal linear damping coefficient (no phase control) as computed by WAMIT (red) and OXPOT (black).

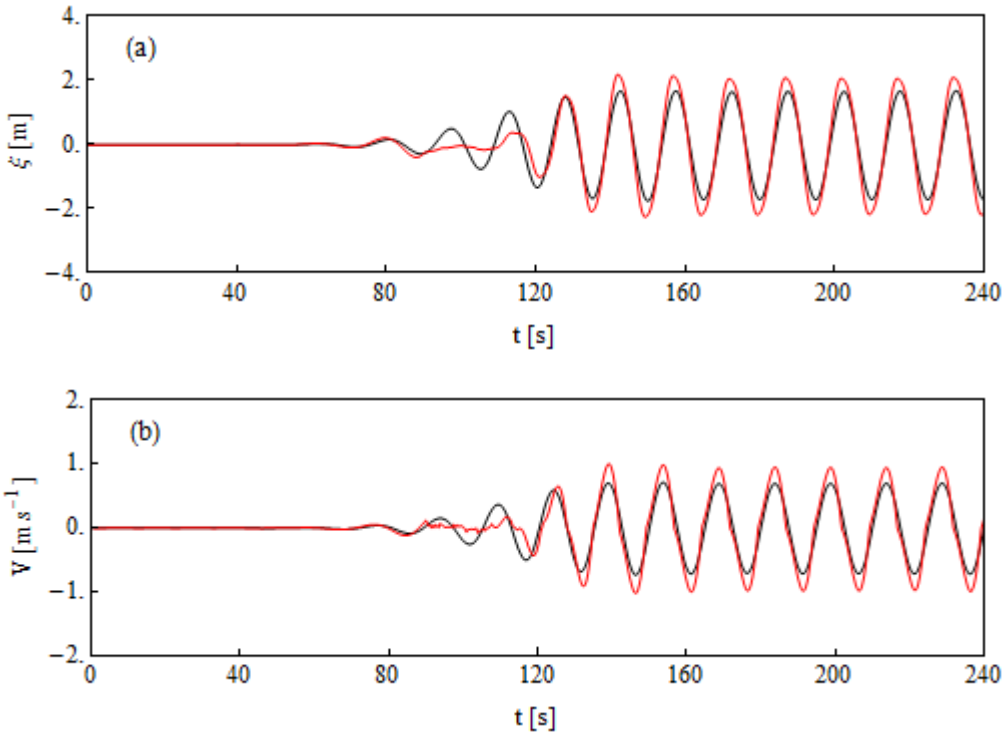

Figure 13: Comparison of the (a) displacement and (b) velocity of the truncated cylinder subject to a Coulomb damping PTO force (red) and linear damping PTO force in regular incident waves of period 15s and height 4m.

One observation worth noting is that the Coulomb damping force is applied before the fully formed incident wave has arrived at the structure because from 90s – 110s the device motion is very small and the velocity changes in an erratic, unsteady manner. This indicates that the exciting force exerted by the incident wave on the device does not have a sufficiently large amplitude to overcome the Coulomb damping force for significant intervals in wave cycle and so motion can only occur, if at all, around the maxima. In this case, the equation of motion of the body should be adjusted to describe the motion of a body close to limiting friction, that is no motion if the hydrodynamic force is, on average, less than the limiting friction and the usual equation of motion with the Coulomb damping term once the sinusoidal amplitude of the hydrodynamic force is sufficiently large to overcome the limiting friction force.

Nevertheless, once the device begins to oscillate after 120s of the simulation, the device subject to the nonlinear PTO force moves with a larger amplitude of motion than the device subject to the linear PTO force and the periodic motion has quite distinct characteristics. In particular, the velocity time-histories differ considerably in both amplitude and form. Firstly, the amplitude of the velocity (and displacement) oscillations are roughly 25% larger for the device moving subject to the Coulomb damping than for the linear damping. Furthermore, there is a clear inflection point in the velocity profile as the device changes direction (i.e. as the signal passes through $v = 0$) so the periodic form of the velocity is quite different from regular sinusoidal oscillations. This sudden change in the velocity profile is due to the applied Coulomb force changing direction when the velocity goes from positive to negative (or vice versa) which results in a discontinuity in the total force on the device and hence a discontinuity in the acceleration. The power extracted from the incident waves by the Coulomb damping force is compared to the linear power take-off in Figure 14. The signals are visually quite similar; however, the mean power extracted by the nonlinear PTO over the final 6 periods of the simulation is $1.1MW$ compared to $1.0MW$ for the linear PTO. This 10% increase can be attributed to the slightly broader form of the power absorption peaks due to the Coulomb damping PTO force observed in the 9 second period simulations.

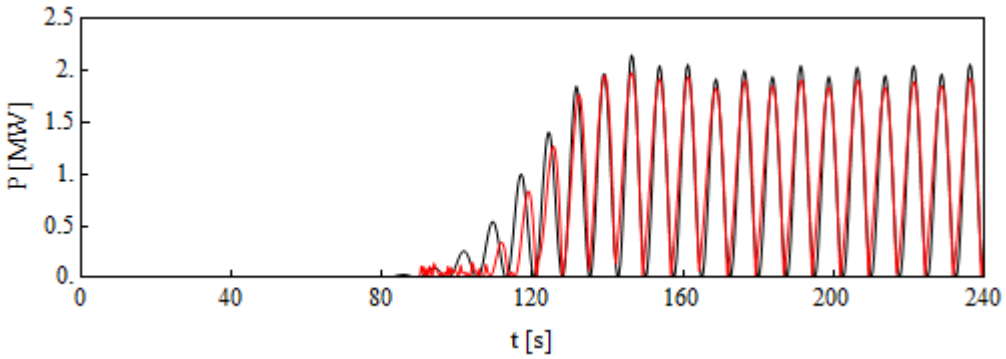

Figure 14: Comparison of the power extracted by the Coulomb damping PTO (red) and linear damping PTO (black) in regular incident waves of period 15s and height 4m

3.4.1 Phase control using reactive (optimal) control and latching (suboptimal) control

To conclude the analysis of the power absorption by the device in regular incident waves with a 15 second period, the effect of phase control on the power captured by the device is briefly analysed. To satisfy the linear resonance condition (17) the system stiffness or reactance must be modified by specifying the PTO restoring force coefficient k to equal $\omega^2(m + a_{33}) - \rho g W$ which in this case gives $k = -1.67\ MN/m$. Negative spring coefficients typically occur for incident wave periods larger than the natural resonant period of the device but are undesirable as they are difficult to implement in reality. This is in addition to the fact that, although the average power due to the phase control or tuning force – kx is zero over one period, the instantaneous power due to this term can be much larger than the damping force. Furthermore, at some instants of the operation cycle the direction of power flow through the PTO can be reversed assuming the phase control force is realised with the PTO. To avoid this problem, sub-optimal phase control by latching is implemented and will be investigated here. First, the optimal power absorption capability of the device is examined with the optimal reactive control.

The velocity and power absorbed by the heaving truncated cylinder tuned to resonance with the incident waves by specification of a PTO force stiffness $k = -1.67MN/m$ as computed by OXPOT and from the linear frequency domain are shown in Figure 15. The linear PTO force damping coefficient is specified to be $0.14MNs/m$ and the average power capture over that last 6 periods is computed to be $4.1MW$. It is clear that the OXPOT solution is approaching the steady state oscillations. However, the large device displacement amplitudes ($\sim 20m$) mean that the OXPOT simulations fail as the resonant steady-state is approached and the bottom of the device reaches the free-surface. Such device motion amplitudes are impractical and this illustrates one of the problems with using a point absorber (an axisymmetric device with small dimensions relative to the incident wave) to absorb incident wave power. To absorb as much energy as possible from the longer incident waves, large device excursions are necessary. Nevertheless, in the next simulations we attempt to achieve resonance with the incident waves by latching control.

As described in section 2.2, latching is a discrete control method which attempts to satisfy the resonant phase condition for optimal power absorption in a sub-optimal manner. In practice, this means that the device is locked in position ('latched') at the instants of zero velocity and released at the instant when the exciting force is back in phase with the velocity. Thus, the device will have zero velocity for intervals during the oscillation cycle of the device at which point no power is absorbed and hence the latching control method is referred to as sub-optimal control.

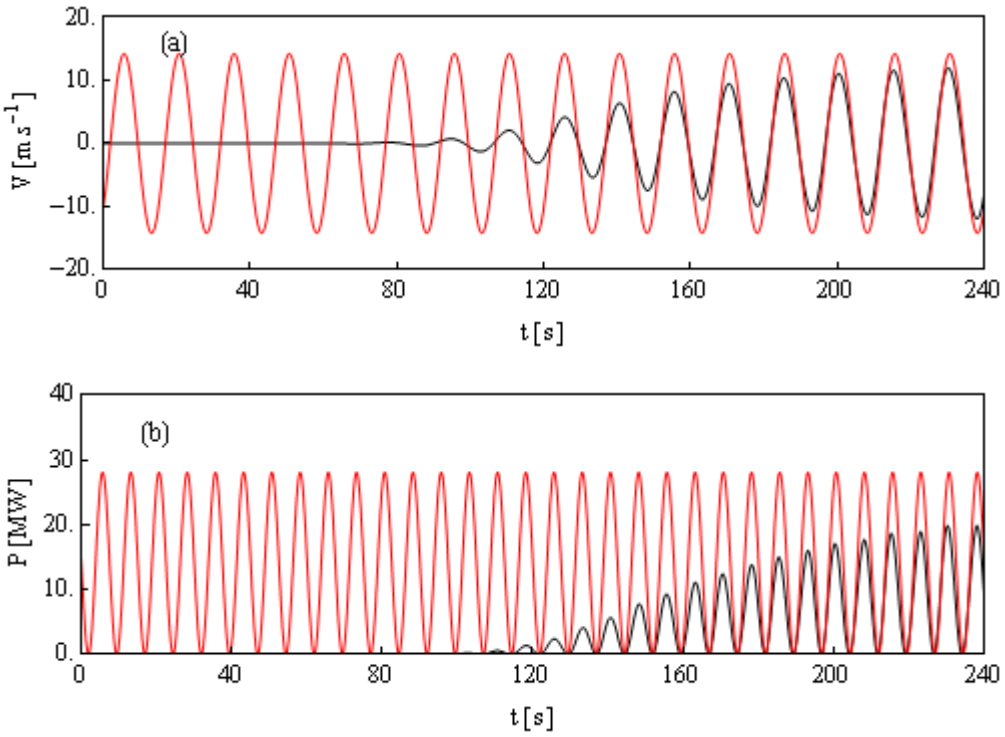

Figure 15: Velocity (a) and power absorbed (b) by the device tuned to resonance with the incident wave ($T = 15s$, $H = 4m$) as predicted by the linear frequency domain theory (red) and OXPOT (black).

To satisfy the phase condition the only control variable that must be optimised is the latching interval or duration, i.e. the time over which the device is held steady before release, and in regular waves it is a predetermined constant. For an incident wave of period 15 seconds and a device of natural period 10.25 seconds, it is clear that the device must be latched for an interval of half the difference (2.375s) between these periods. The same computational domain used for the power take-off simulations was used for the latching control investigation. Initially, no damping force was imposed on the device motion in order to illustrate the basic effects of the latching mechanism. Figure 16 illustrates the magnification of the system response achieved by using latching control to achieve resonance. The steady state for the oscillations is not reached during the simulation and the amplitude of the response continues to grow – this causes convergence difficulties for OXPOT and the latching control simulation diverges before the prescribed end of the simulation. Imposing a PTO damping force should, however, reduce the system response and the power capture simulations remain stable. To illustrate how the velocity and exciting force are kept in phase by the latching mechanism, it is useful to show the velocity of the device in the latched simulation alongside the exciting force as is done in Figure 17.

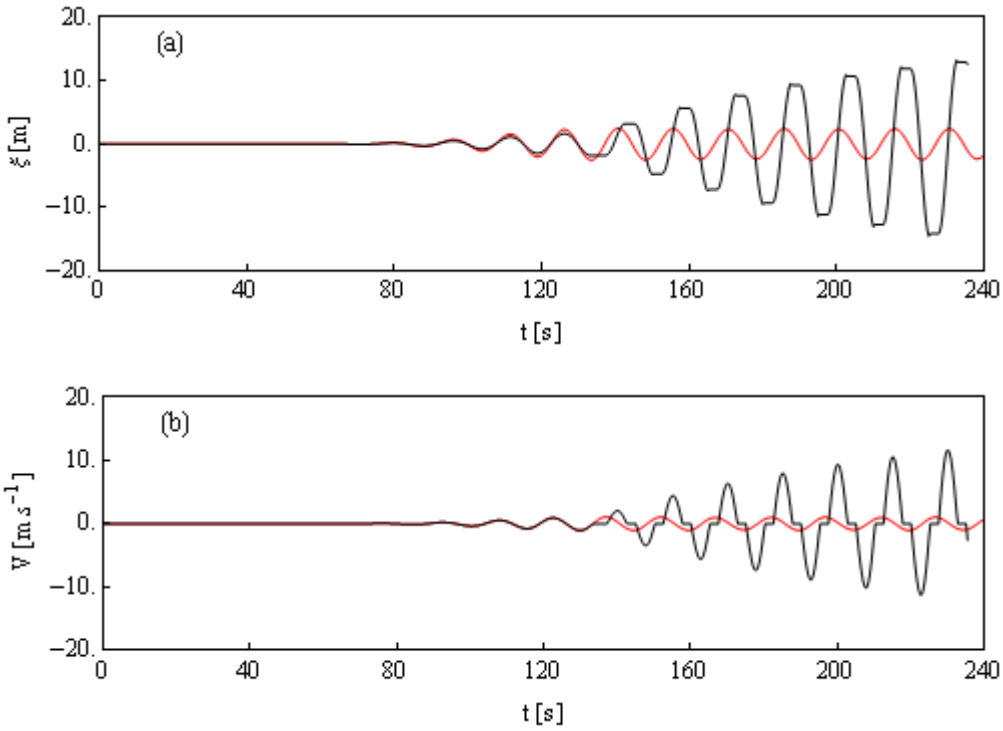

Figure 16: Uncontrolled (red) and latching controlled (black) device displacement (a) and velocity (b) in regular waves of period 15 seconds.

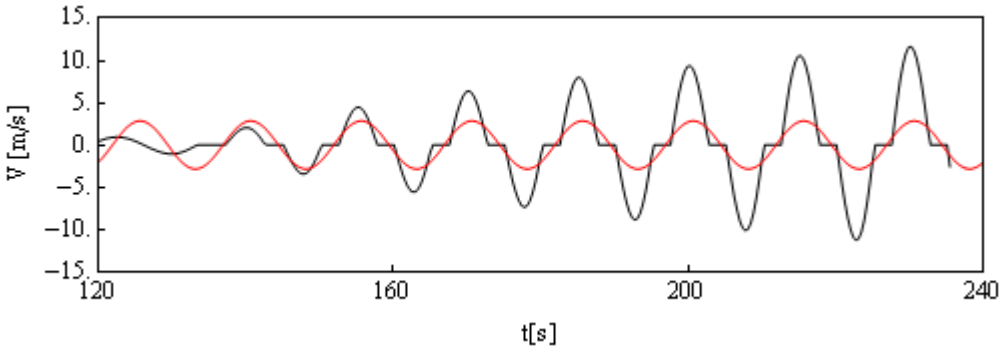

Figure 17: Velocity of the device with latching control (black) and the exciting force on the device (red).

Having demonstrated that the latching interval $T_L = 2.375s$ yields resonant growth of the device motion it can now be shown how this phase control benefits the power absorption performance of a wave energy device. Two different linear power take-off forces are considered, the first corresponding to the optimal damping coefficient for a device operating without phase control ($\gamma = 4MNs/m$) and the second corresponding to the optimal damping coefficient for a device tuned to resonance by optimal (reactive) phase control ($\gamma = 0.14MNs/m$). The optimal damping for the device responding without phase control is an order of magnitude larger than that for the case of reactive phase control and so it can be expected that motions will be significantly smaller for this stronger damping case.

For the larger of the linear PTO force, the velocity and instantaneous power absorbed are shown in Figure 18. The linear damping force is applied after $t = 7.5\,T \simeq 112.5$ and the latching algorithm after the 8 period. Once latching begins, the device quickly settles into steady-state periodic oscillations with relatively small amplitudes (the maximum excursion of the device is less than $1.5m$ as shown in Figure 18 (a)). Such small amplitude oscillations are desirable from a WEC design perspective but imposing such a strong damping force may not be practical. The average power extracted over the last 5 periods of the simulation is $1.6\ MW$. This may seem relatively small compared to the size of the instantaneous power absorbed peaks; however, it must be borne in mind that the device does not extract power for approximately 1/3 of the oscillation cycle during the latching phase. It is for this reason that latching control is referred to as a suboptimal phase control strategy. The average power capture for the unlatched device (without any phase control) subject to the same PTO force is $1.0MW$ and so a significant (+60%) increase in power capture is realised through latching. Further increases may be possible – a second linear PTO force is examined next.

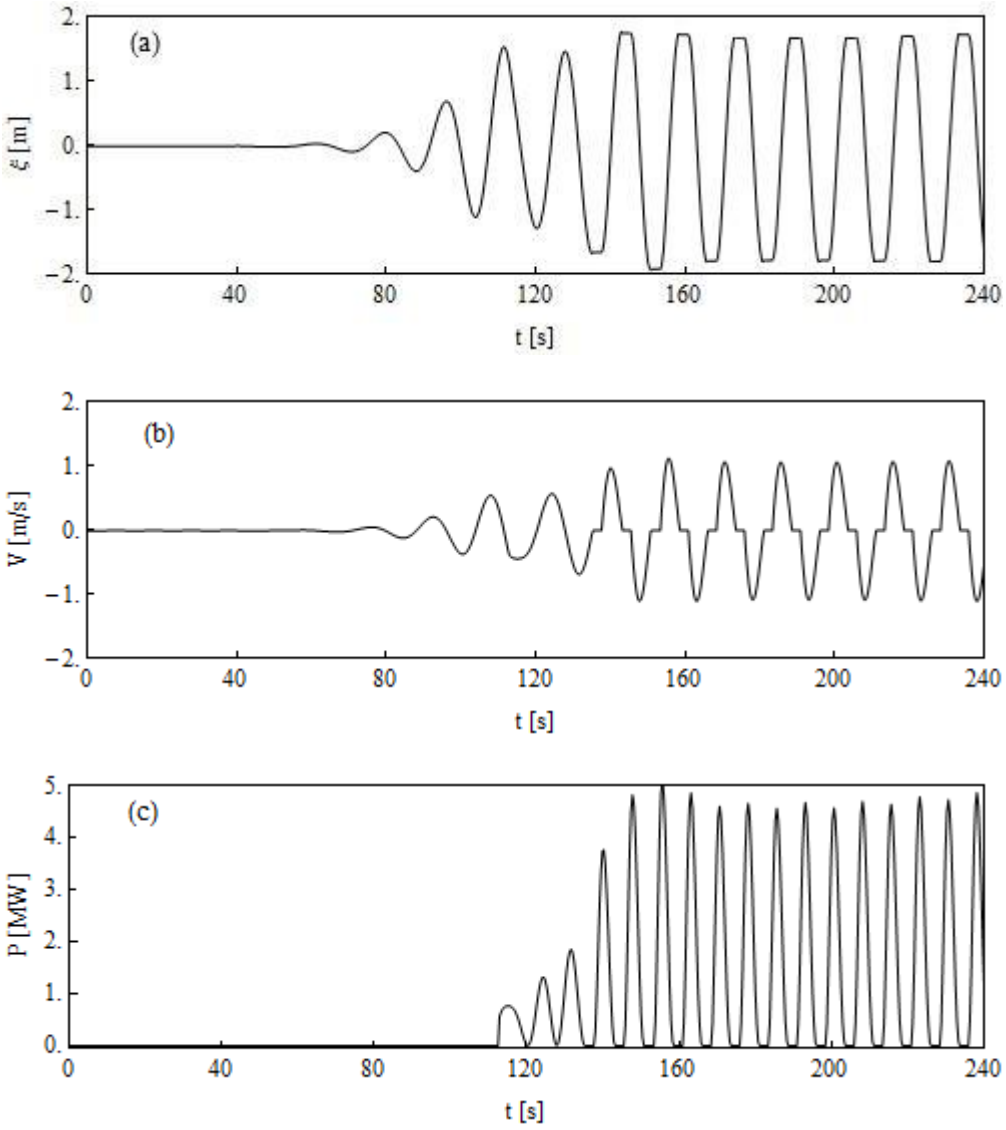

Figure 18: (a) Displacement, (b) velocity and (c) instantaneous power absorption of the device responding to the incident regular wave with latching and power take-off applied from $t = 112s$ for the linear power take-off force coefficient $\gamma = 4MNs/m$.

By setting the linear PTO damping force coefficient to be significantly smaller than in the previous simulation, it should be possible to improve the power absorption performance of the device through a reciprocal increase in the velocity amplitudes. The velocity and instantaneous power absorbed for the device operating with a linear PTO damping coefficient of $\gamma = 0.14MNs/m$ (which will be referred to as the weakly damped case) are shown in Figure 19. It is immediately obvious that the steady-state velocity amplitudes have increased considerably due to the decrease in the damping force and the motion evolves in the same manner as the motion of the latched device with no PTO force; however, the growth in the oscillation amplitudes decreases towards the end of the simulation. The displacement amplitude of the device with weak damping is approximately three-quarters of the draft. By considering the instantaneous power absorbed, it is evident that the latched device subject to a weak linear PTO damping linear has power absorption capabilities greater than the strongly damped latched device and less than the weakly damped device with optimal phase control. The rate of increase in the instantaneous power absorbed for the latched device is quite similar to that of the device with reactive control. In an attempt to quantify the power extraction properties of the latched, weakly damped device, the average power capture over the final 6 periods of the simulation was computed to be $2.80MW$ which is 75% greater than in the case of strongly damped latched motion. A summary of the average power capture results for all the simulations involving T=15.0s incident waves analysed here is presented in Table 4.

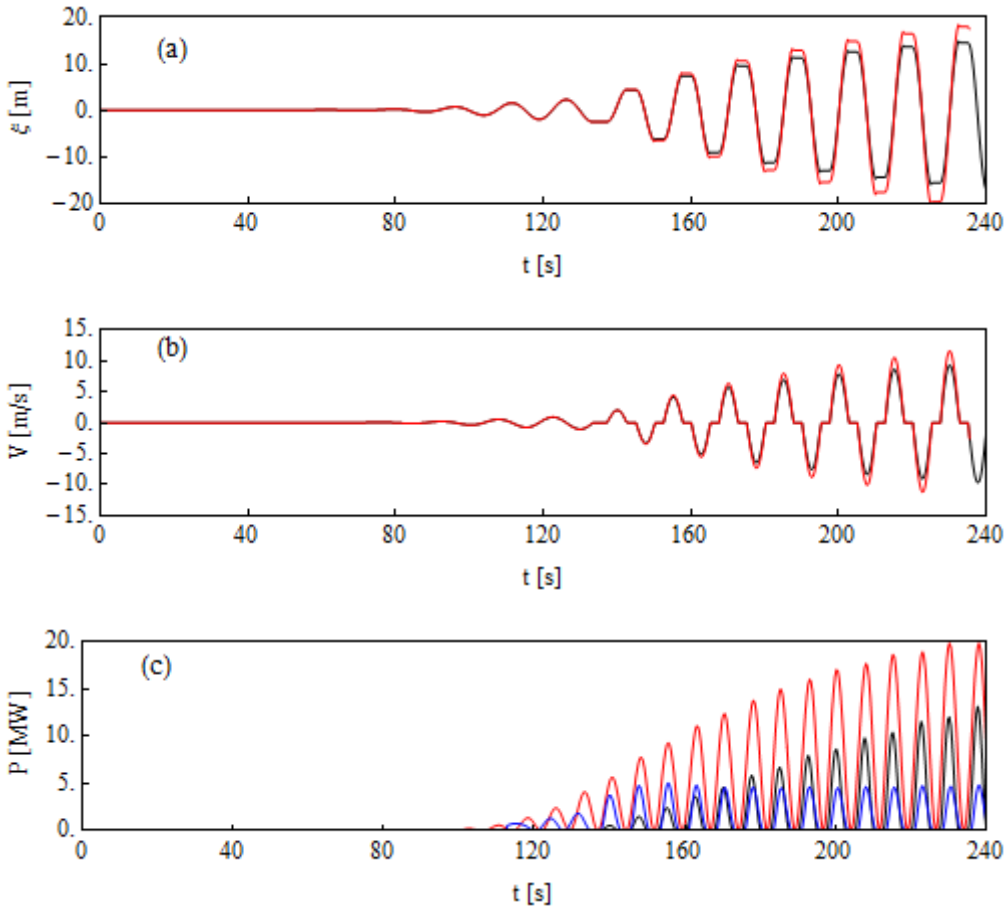

Figure 19: Comparison of the displacement (a) and velocity (b) of the device subject to a linear damping PTO force (black) and undamped (red) and the instantaneous power absorbed (c) for the device with latching control (blue) and damping coefficient $\gamma = 4.0MNs/m$, with latching control and damping $\gamma = 0.14MNs/m$ (black) and with optimal phase control (red) for $\gamma = 0.14MNs/m$.

	PTO damping force		PTO Stiffness	Average Power
PTO, phase control	$\gamma\ (MNs/m)$	$\mu\ (MN)$	$k\ (MN/m)$	$P_M(MW)$
Linear	3.99	–	0	1.00
Nonlinear	–	1.94	0	1.10
Linear, reactive	0.14	–	−1.67	4.1
Linear, latching	3.99	–	0	1.6
Linear, latching	0.14	–	0	2.8

Table 4: Summary of the average power capture for the simulations of power take-off for regular incident waves of period T=15.0s.

3.5 Linear and quadratic power take-off

In WG1 WP1 D3 two different explicit PTO models were investigated using the linear time-domain model being developed by GH (WaveDyn). The first order explicit PTO model was designed for implementation in both the frequency domain analysis and also the time-domain simulations. The PTO force expression followed the typical spring damper form (5) and the device motions are controlled by tuning the spring coefficient k and the damping coefficient γ, where power take-off is also achieved through the damping term. The time-domain model allows much more complex models of power take-off (e.g. Coulomb damping force) and, to illustrate the increase in generality, the results of a simulation of power take-off involving a damping force with a quadratic dependence on velocity are shown in section 6.4 of WG1 WP1 D3. The second order explicit PTO model implements control and PTO forces of the general form

$$F_{PTO} + F_{CON} = -\gamma_1\,\dot{x} - \gamma_2\dot{x}|\dot{x}| - k_1 x - k_2 x|x| - E \tag{32}$$

where γ_1 and γ_2 are the linear and quadratic damping coefficients, k_1 and k_2 are the linear and quadratic stiffness coefficients and E is a control load. However, in the simulation involving the second order PTO model described in WG1 WP1 D3 only the quadratic damping term was retained and no control of the phase was attempted so that the total PTO force was simply

$$F_{PTO} = -\gamma_2\dot{x}|\dot{x}|\,. \tag{33}$$

Furthermore, in the simulation of linear power take-off the PTO force was $-\gamma_1\dot{x}$. Here, we attempt to reproduce both sets of results, for linear and quadratic power take-off forces, using OXPOT and compare the resultant device motions and power capture just as in Figures 6.2 – 6.5 in WG1 WP1 D3.

The incident wave climate and device geometry specifications are as follows: regular incident waves of amplitude $A = 1m$ and angular frequency $\omega = 0.7\ rad/s$ ($T = 8.98s$) in water of depth $h = 40m$ are incident on a floating truncated cylinder of radius $a = 10m$ and draft $d = 20m$. The mass of the cylinder is uniformly distributed; the cylinder is neutrally buoyant at rest and moves in heave only. The linear damping coefficient has the value $2MNs/m$ and the quadratic damping coefficient the value $6MNs^2/m^2$ – these values were selected so that the device responses would be similar despite the difference in the PTO force profiles.

In the OXPOT simulations, a numerical wave tank containing the device must be generated with one end wall as the wavemaker. Therefore, the side and end walls, wetted body surface, free surface and subdomain interfaces (domain decomposition is used) must be discretised using structured

quadrilateral and unstructured triangular elements with quadratic variation. Given the symmetry of the problem, the solution is only solved on one half of the total domain. The total domain and boundary discretisations are shown in Figure 20. It should be noted that all lengths have been non-dimensionalised by the depth h and that in the simulations all times are non-dimensionalised by $\sqrt{gh}$. The wavelength of the incident wave in this non-dimensional formulation is approximately 3 units and given that the half-width of the domain is just 2.5 units it is clear that artificial reflections from the side walls will affect the results.

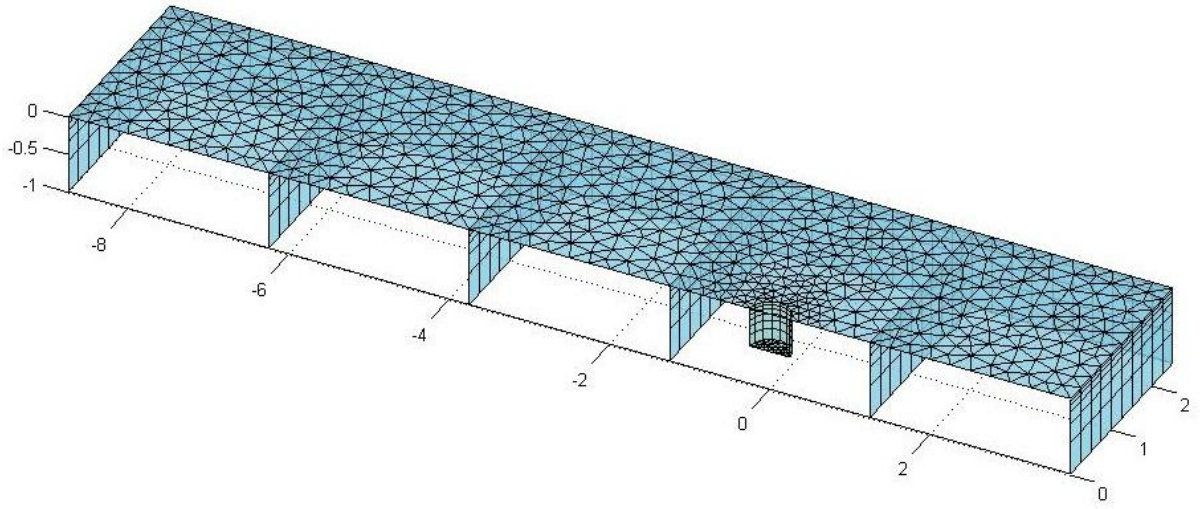

Figure 20: Discretised domain boundary for simulations of linear and quadratic PTO forces.

The details of the discretisation of this domain boundary are given here because they have not been described before in previous deliverables. The domain shown in Figure 20 is decomposed into 5 different subdomains. In each of the subdomains not containing the device there are 180 quadrilateral elements on the side walls and interfaces and 238 triangular elements on the free-surface. Similarly, the subdomain containing the device has 228 quadrilateral elements on the walls, interfaces and vertical cylinder surface and 379 triangular elements between the truncated and free surface. In total there are 2279 elements corresponding to 6259 nodes. The interactions are simulated over 20 periods with time-steps of one-fiftieth of a period and the incident wave is generated with a wavemaker ramp imposed for the first 4 periods. The last subdomain to the right of the structure has a damping zone imposed on the free-surface to absorb the transmitted waves.

The displacement, velocity, power take-off force and power capture over the course of the OXPOT simulations for the linear and quadratic PTO forces are shown in Figure 21 with the results of the linear time-domain model from WG1 WP1 D3 for the quadratic PTO force also included. The comparison between the response of the device subject to both linear and quadratic PTO forces is very similar to that for the linear time-domain model (see Figures 6.3 – 6.5 in D3). Although there is a significant difference in the peak power absorbed as predicted by OXPOT and the linear time-domain model, the velocity profiles are very similar and the difference at the extremes may be attributed to a combination of nonlinear hydrodynamic effects and side wall reflections.

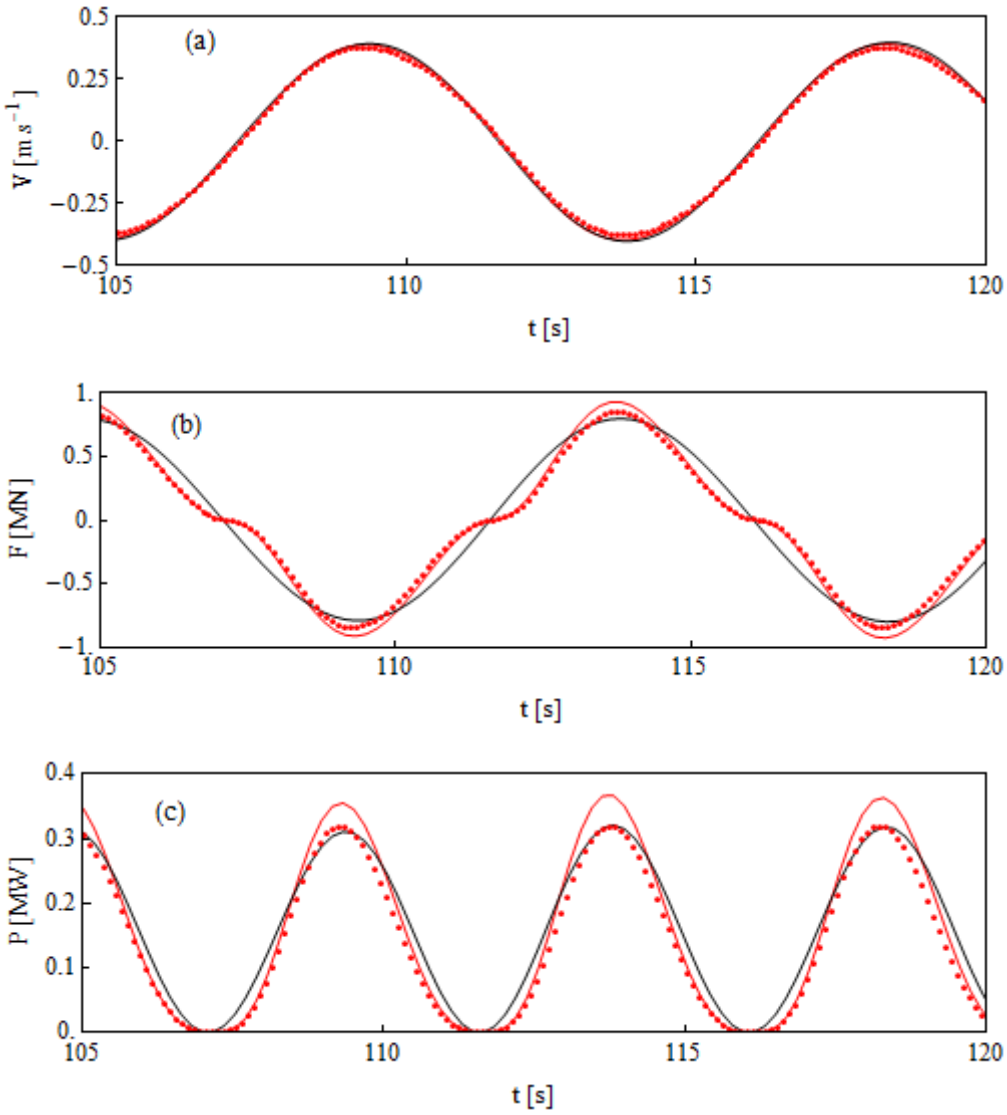

Figure 21: (a) Velocity of device; (b) PTO force on the device and (c) power captured by the device over a short duration of the two OXPOT simulations featuring the linear PTO force (black) and quadratic PTO force (red) and for the linear time-domain simulation from WG1 WP1 D3 (dotted red).

4 ARRAY OF CONTROLLED DEVICES IN REGULAR SEAS

The power absorption capabilities of arrays of heaving axisymmetric devices in regular seas have been investigated using many different linear models for the interactions between the cylinders, including the point absorber theory (Budal & Falnes, 1980) and (Thomas & Evans, 1981), the plane wave approximation (McIver, 1994) and more recently the full linear diffraction theory (Siddorn & Eatock Taylor, 2008). In most of the investigations, the device motions are assumed to be optimal so that the velocities satisfy the condition for optimal power for an array (21) and the mean power capture is given by (22) and the effects of changes in configuration on the power capture are examined. The simple point absorber theory approach yields results valid only for arrays of large inter-device spacing and devices of sufficiently small dimensions relative to the wave frequency while the full diffraction theory is valid for all spacings including relatively compact arrays. Nevertheless, in all cases in long waves the optimal device motions require large motions which would violate the assumptions of the linear theory.

In the case of the OXPOT simulations, the underlying hydrodynamic model is fully nonlinear and so even for large motions (relative to the draft of the device) and locally large waves the results are consistent with the underlying theory. However, in the simulations that follow the operation of the devices with sub-optimal control is of more interest than the operation of the devices at resonance. Therefore, the devices in most cases are not tuned to resonance and the focus will be on the implementation of amplitude control via linear and nonlinear PTO forces. Nevertheless, some simulations of cylinders tuned to single body resonance are considered. The advantage of considering sub-optimal control is that the large displacement amplitudes associated with resonance and which are difficult to realise in full scale WEC operations do not arise. Therefore, we seek to examine the power capture of the devices operating with sub-optimal control in an array and to compare to a single device absorbing in isolation with identical power take-off forces. Although the multiple body absorption theory allows us to compute optimal damping and stiffness coefficients for each device in an array (see section 7.2 of (Falnes, 2002)), it is more straightforward to choose identical amplitude control for each device. Furthermore, direct comparisons with the behaviour of a device in isolation and in an array are possible.

4.1 Array configuration and computational domains

A schematic of the device array configuration is shown in Figure 22. The device geometries are all identical to single truncated cylinder considered in the last single body section (the exact specifications are in Table 1) and are floating in water of depth 80m which is four times the radius. Only one incident wave direction is considered with heading $\beta = 0$ and one spacing $d = 6a$ so that the cylinders are three diameters apart. As discussed in WG1 WP1 D9, these restrictions are necessary to minimise the cost of the already computationally expensive simulations. The symmetry of the solution perpendicular to the direction of the incident wave can be exploited to further minimise computational times. If the x-axis is aligned along the incident wave direction with origin at the centre of the square formed by the four cylinder centres and the y-axis pointing towards cylinder 1 and 2 then it is only necessary to solve for the upper half ($y > 0$) of the domain encompassing cylinders 1 and 2 only. The responses of cylinders 3 and 4 and the lower half ($y < 0$) of the free-surface is then given by symmetry. In the simulations, the incident wave excites the motion of the devices which respond independently and are controlled by a PTO force modelled as a linear spring and linear/nonlinear damper combination. In order to assess the results, comparisons

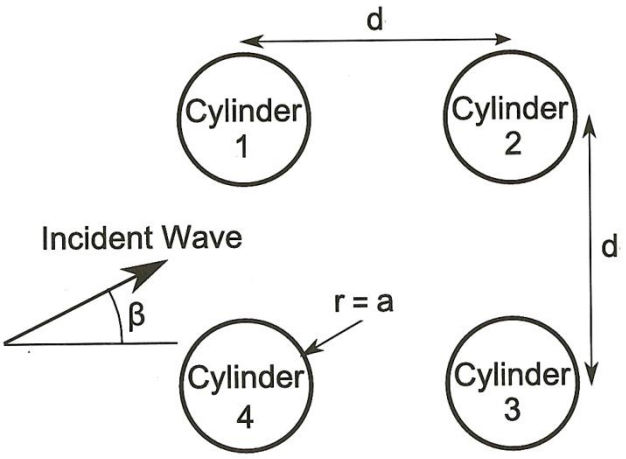

Figure 22: Four device array configuration for cylinders of radius a spaced a distance d apart.

with the uncontrolled motions of devices in arrays and the controlled motion of a single device are made.

Two regular waves with different incident wave periods are investigated here, the first with period 9 seconds and the second with period of 15 seconds and both waves have amplitudes of 2 metres. These two wave periods are of most interest because the devices naturally operate away from resonance but can be tuned to resonance if required. Furthermore, the waves are chosen so that there are waves with frequency higher than the natural device frequency ($T = 9.0s$) and also lower than the natural device frequency ($T = 15.0s$). The incident wavelengths differ considerably, with $\lambda \simeq 126m$ in the former case and $\lambda \simeq 320m$ in the latter case, and so the computational domains are also quite different and will be described and illustrated next.

Scaling all lengths by the water depth, it can be seen that the incident wave with a period of 9 seconds has a wavelength of $\lambda = 1.57h$ and the circumference of the cylindrical device is approximately $0.79h$ so that the circumference-to-wavelength ratio is approximately one half. On the other hand, in the case of the wave with period 15 seconds the wavelength is $\lambda = 4.02h$ and the corresponding circumference-to-wavelength ratio is approximately one fifth. Therefore, the required fineness of the mesh around the device to resolve first and second order waves will be much coarser for the 15 second wave. In the discussion of the details of the computational domains to follow, the lengths are assumed to have been non-dimensionalised, i.e. $h = 1$.

The total computational domain for incident wave of period 9 seconds is shown in Figure 23 and the exact specifications are summarised in Table 5. The domain is divided into 6 subdomains of length 1.333 and width 1.5. The triangular free-surface elements in the subdomains not containing the cylinders typically have a side-length of 0.12 while around the body, where the mesh is finest, the elements have typical side-lengths of 0.044 corresponding to 36 elements per wavelength at the cylinder. For the longer incident wave, the computational domain and mesh is significantly different because of the relative size of the cylinder to the incident wavelength. The domain is of total length 18.0 and is subdivided into 5 equal subdomains of length 3.6 and width 3.8. Note that for both incident waves the domain half-width is less than one wavelength and thus the domains are

relatively narrow. In the subdomains not containing the cylinder, the triangular free-surface elements have side-lengths of approximately 0.25 which is more than twice that of the shorter wave case. The circumference of the cylinder is divided into 10 elements of arc length 0.08 which corresponds to 50 elements per wavelength. Therefore, although in absolute terms the $T = 15.0s$ mesh is much coarser than for the $T = 9.0s$ case as can be seen in Figure 24, relative to the incident wavelength the mesh around the cylinders is substantially finer for the $T = 15s$ incident wave than it is for the $T = 9s$ wave. The number of nodes and elements does not vary greatly between the two simulations because of the larger domain required for the longer wavelength case. Each simulation lasts for 16 periods with time steps of $0.025T$ and $0.02T$ for the wave of period 9 seconds and 15 seconds, respectively. Typical computational times are approximately 160 hours on a single processor.

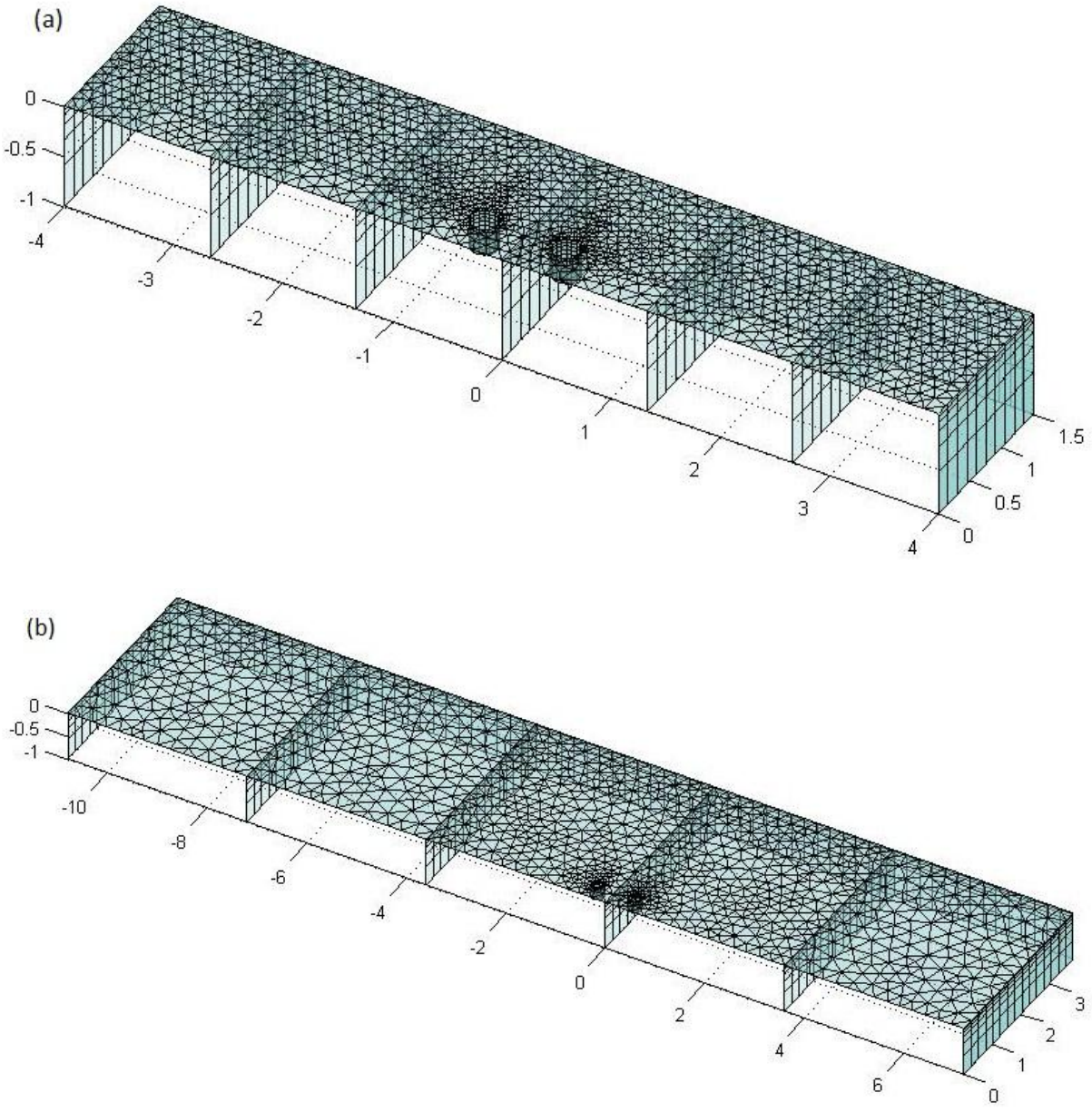

Figure 23: Meshing of computational boundary for (a) the regular incident waves of period 9 seconds and (b) of period 15 seconds.

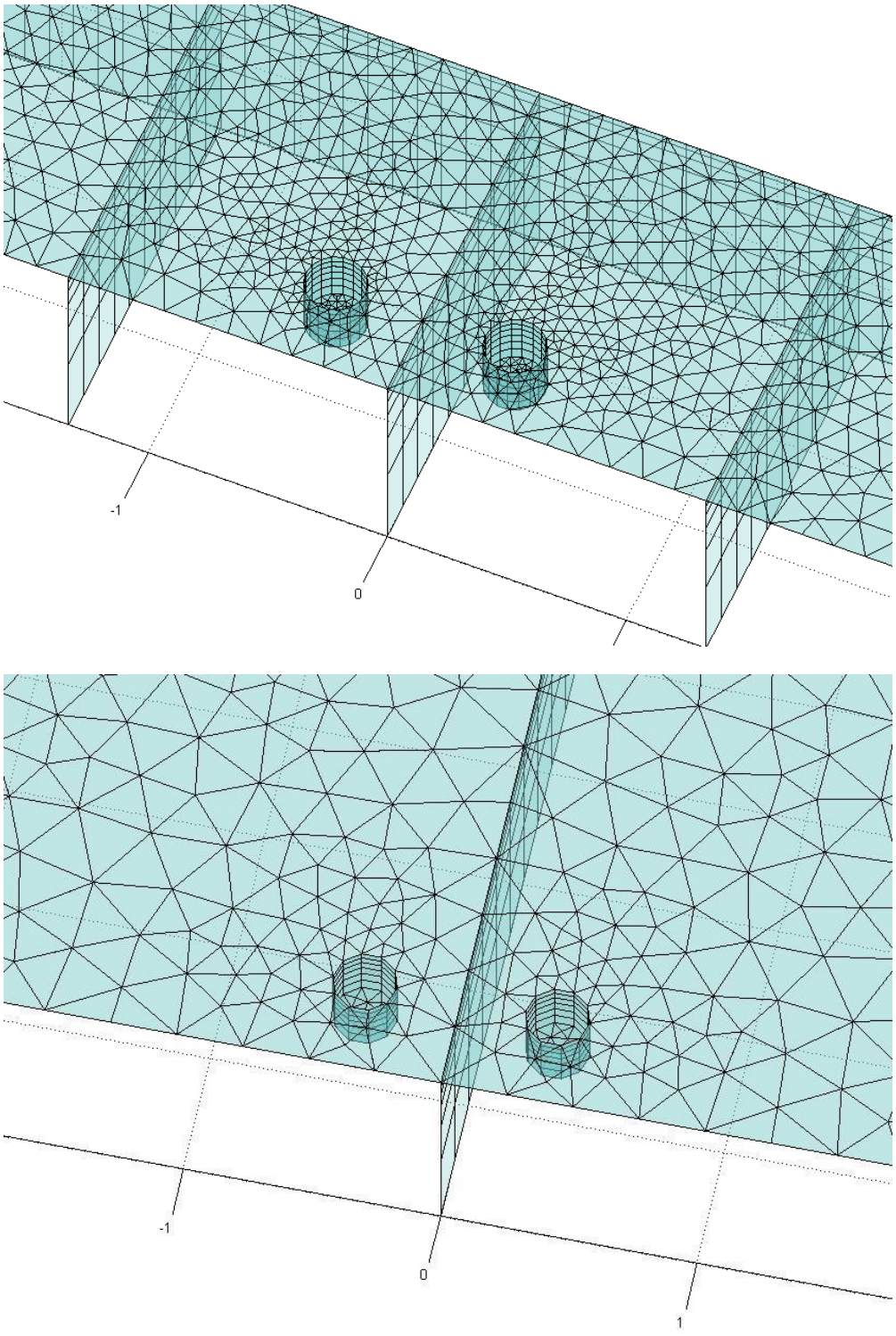

Figure 24: Zoomed view of elements around cylinders for the 9 seconds (above) and 15 seconds (below) incident waves to emphasise different meshing approaches necessary.

Wave Period	Comp. Domain		Subdomain intervals		Body elements		Total	
	(L, L_{SUB})	W	n_x	n_y	N_{CURVE}	N_{TRUNC}	Elements	Nodes
$(9s, 4m)$	(8.0,1.33)	1.5	10	13	(18×6)	136	4248	11658
$(15s, 4m)$	(18.0, 3.6)	3.8	14	15	(10×6)	32	3908	10891

Table 5: Computational domain specifications and computational domain boundary discretisation properties for the two incident waves considered.

4.2 Simulation results

4.2.1 $T = 9.0s, H = 4.0m$ incident wave simulations

The first simulation for the power absorption by an array of controlled devices in regular waves involved applying an identical linear damping PTO force on each cylinder to control the motion amplitude without imposing any phase control or resonance tuning. The linear damping coefficient was chosen to be the optimal value for a single body in incident waves of period 9 seconds oscillating without phase control, i.e. $\tilde{\gamma} = 0.0069$ in non-dimensional terms or $\gamma = 1.26MNs/m$ in SI units. The motion of the devices subject to the amplitude control is compared to the uncontrolled motions of the devices (as computed and presented in WG1 WP D9) in Figure 25. The comparisons are very similar to those between the single uncontrolled and controlled cylinder shown in Figure 2(a) in so far as the damping suppresses the excitation of the transient resonant mode and the oscillations settle to a steady state at the wave excitation frequency.

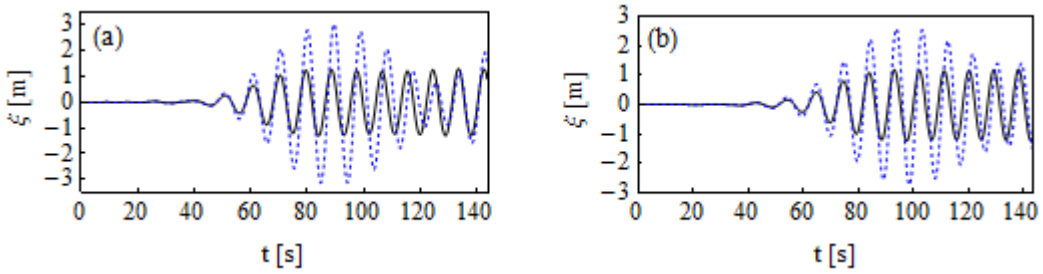

Figure 25: Comparison of the uncontrolled (blue, dashed) and controlled (blue) motion of (a) cylinder 1 and (b) cylinder 2 in the four body array configuration.

When comparing the motion or power absorption performance of the array devices with the single device in isolation, the positions of the cylinders/devices relative to the wavemaker in the simulations are important. For example, the cylindrical devices in Figure 23 (a) are centred at $(x, y) = (\pm 0.375, 0.375)$ where the domain origin is a distance 4.0 from the wavemaker. Thus, cylinders 1 and 2 are a net distance of 3.625 and 4.375 from the wavemaker, respectively. However, in the single body simulations the cylinder is located a distance of 4.375 from the wavemaker. Therefore, the operation of cylinder 2 in the array can be compared directly to that of the single device in isolation and any differences will be due to the presence of device 1 in the device array

simulations. Cylinder 1 is a distance 0.75 or almost half a wavelength in front of cylinder 2 in the incident wave field and hence the motion response and power absorption signals lead those of cylinder 2 by 180^o. This is best illustrated by comparing the performance of the cylindrical devices both to each other and to the single device in isolation as is done in Figure 26.

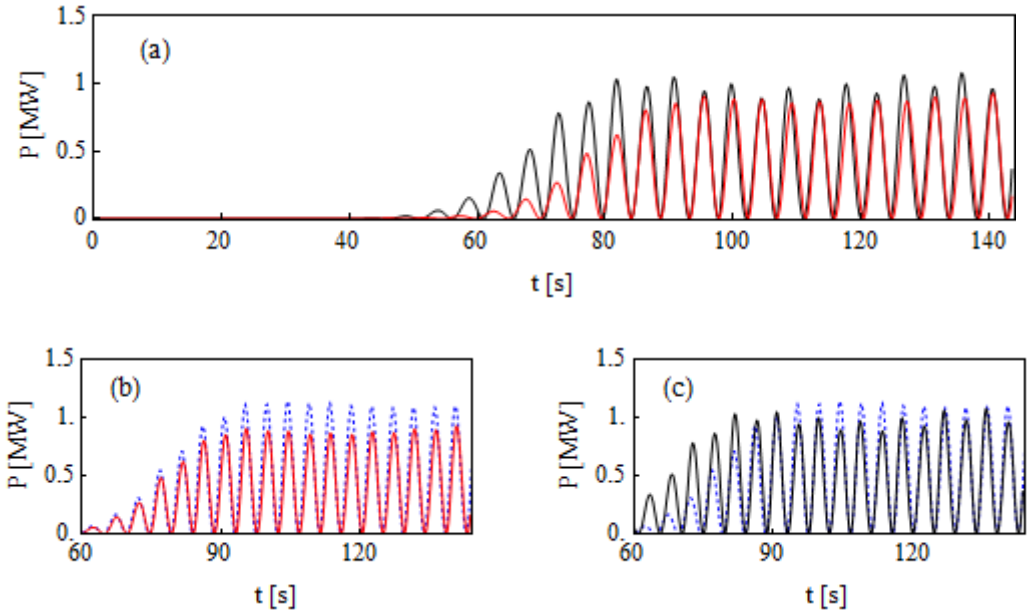

Figure 26: Power extracted by device 1 (black) and device 2 (red) in an array with a spacing three diameters compared to power extracted by an isolated device (dashed blue) in regular 9s waves.

In Figure 26 (a), the power absorption performance of both device 1 and 2 are plotted over the complete duration of the simulation. It is clear that device 1 arrives at steady state first, as expected, and that it absorbs on average more wave energy than device 2. This should also be expected as not all the incident wave energy is available to device 2 due to its position behind device 1 relative to the incident wave front. Furthermore, a single device in isolation outperforms each device in the array as evidenced by Figure 26(b) (device 1) and Figure 26(c) (device 2) – this is to be expected because the linear damping coefficient γ was optimised for a single cylinder without phase control. If the linear damping coefficients were optimised for this particular array configuration then it might be possible to achieve a better performance for one or both of the cylinders relative to the device in isolation. Over the last 5 periods of the simulation, the average power capture of device 1 and device 2 is $0.51MW$ and $0.46MW$, respectively, whereas the single device in isolation extracts $0.57MW$ over the same period for the corresponding single device simulation.

Device response and performance in the square array of devices spaced three diameters apart was also analysed with nonlinear (Coulomb damping) power take-off. The constant applied force μ was chosen to have the value $1.09MN$ corresponding to the approximate root mean square value of the linear damping force with damping coefficient $\gamma = 1.26MNs/m$. In this simulation, the Coulomb damping force is applied only when the main regular component of the incident wave has arrived so that during the build-up to regular waves, while the small amplitude long waves at the wave front impinge on the devices, the devices are allowed to heave in an uncontrolled manner. In implementing the Coulomb damping force, the force is applied for device 1 after 7 periods and for device 2 after 8 periods of the simulation. Therefore, the instantaneous power absorbed by device 1

(2) is only non-zero from 7 (8) periods into the simulation from when the Coulomb damping power take-off is applied. In order to compare the motion of device 1 with that of the single device in isolation, the phase of the signal for the single device is shifted by π so that the troughs and crests align. It is clear from Figure 27 (a) and (b) that for both devices the responses are reduced by the presence of surrounding devices and from Figure 27 (c) that the power output from each device is less than for the single device in isolation.

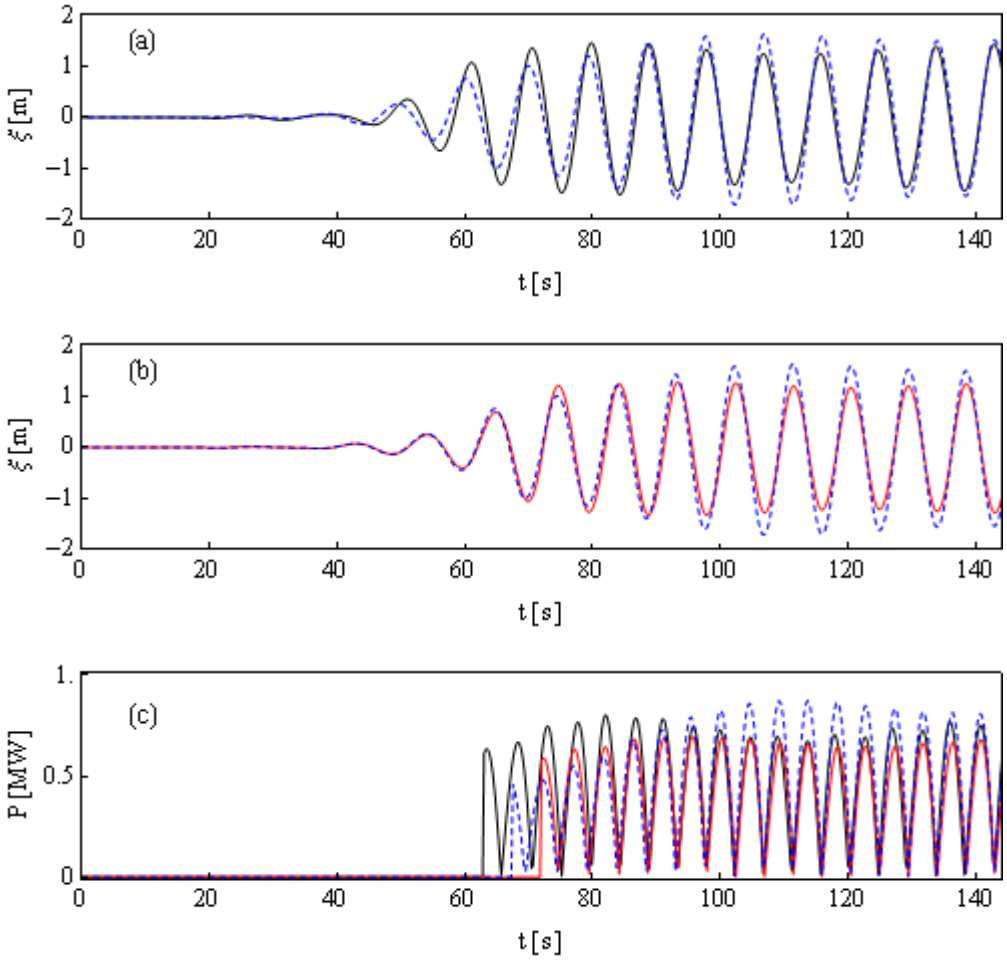

Figure 27: (a) Displacement of device 1 (black) compared to a single device in isolation (dashed, blue); (b) displacement of device 2 (red) compared to a single device in isolation (dashed, blue) and (c) the instantaneous power absorbed by devices 1 and 2 and the single device in isolation.

The operation of the devices in the array for stiffness k giving resonance in the single body case was also simulated. The displacements of the devices are compared to the single body displacement in Figure 28 from 60s into the simulation onwards, where the device motion is significant. The motion of device 2 in the array is very similar to that of the single body as expected although the phase and amplitude are slightly different (smaller in the case of the amplitude) due to the presence of radiated waves from device 1. The steady state solutions are expected to have differences in the amplitude and phase also. Furthermore, the phase of the motion of device 1 is approximately π ahead of the single device motion. In the power capture comparisons, it is more straightforward to consider together device 2 and the single device in isolation because the device motions in these

cases have been excited by the same wave over the same period of time. Given that device 1 is located nearest to the wavemaker its displacement will have evolved farther towards the resonant steady state than device 2 or the single device in isolation both of which are located the same distance from the wavemaker. If the simulation time for the resonant motions and power take-off of the devices in the four body array was specified to be sufficiently long for steady-state oscillations to occur then it is possible that prior to the onset of steady-state, if the amplitudes of the motion became too large and approached the draft of the devices, the OXPOT solution would fail to converge just as in the single body case for incident wave frequency equal to the natural device frequency. Nevertheless, the power capture during the resonant growth in the displacement amplitude is worth considering. In particular, over the last 5 periods of the simulation, the average power capture of device 2 is $0.69MW$ and for the single device in isolation it is $0.89MW$ illustrating the effect of the leading device on the incident energy available to the second device.

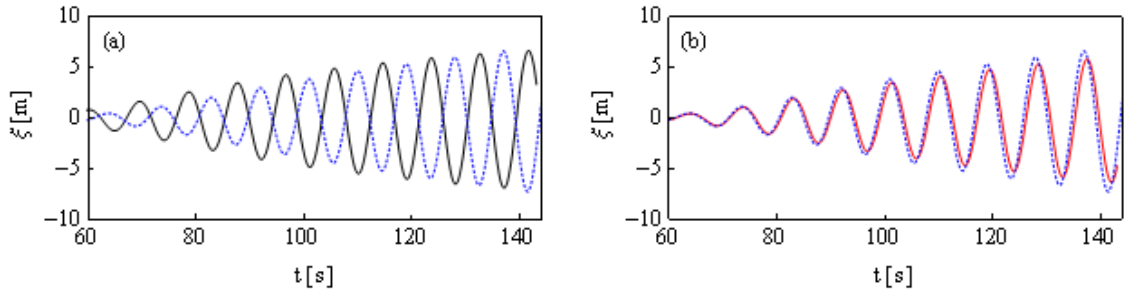

Figure 28: Displacement of (a) device 1 (black) and (b) device 2 (red) in the array of devices compared to the single device displacement for identical incident waves.

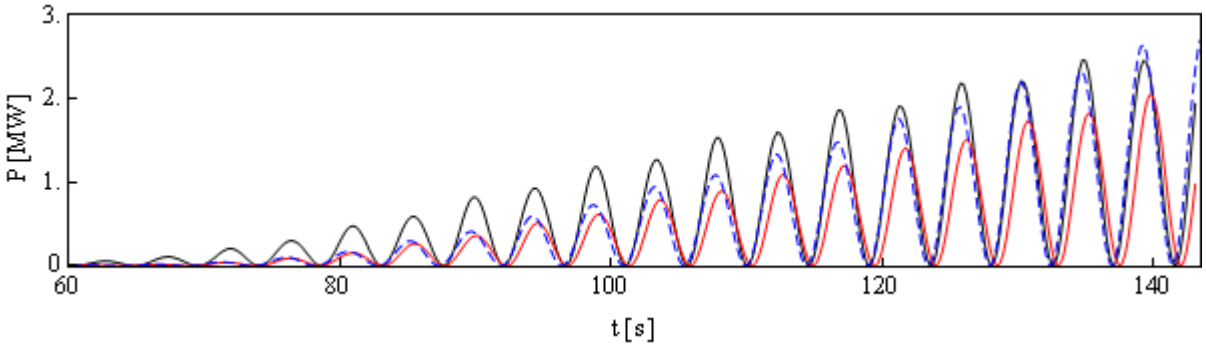

Figure 29: Power extracted from the incident wave by device 1 (black), device 2 (red) and the single device in isolation (dashed blue).

4.2.2 $T = 15.0s, H = 4.0m$ incident wave simulations

The response and power take off of the devices in the square array of four devices of side length three diameters was also simulated in the case of the long wave of incident period T=15.0s. Before analysing the results, it is useful to note that the device dimensions relative to the wavelength are very small – the typical parameter used is $(2\pi/\lambda)r$ where r is the device radius and in this case it takes the value 0.195. In the case of the $T = 9.0s$ waves the same parameter equals 0.5. Furthermore, just as in the previous analysis, the phase of the displacement time-history signal for the isolated device is shifted to allow straightforward comparisons of the steady state amplitudes of the devices in the square array.

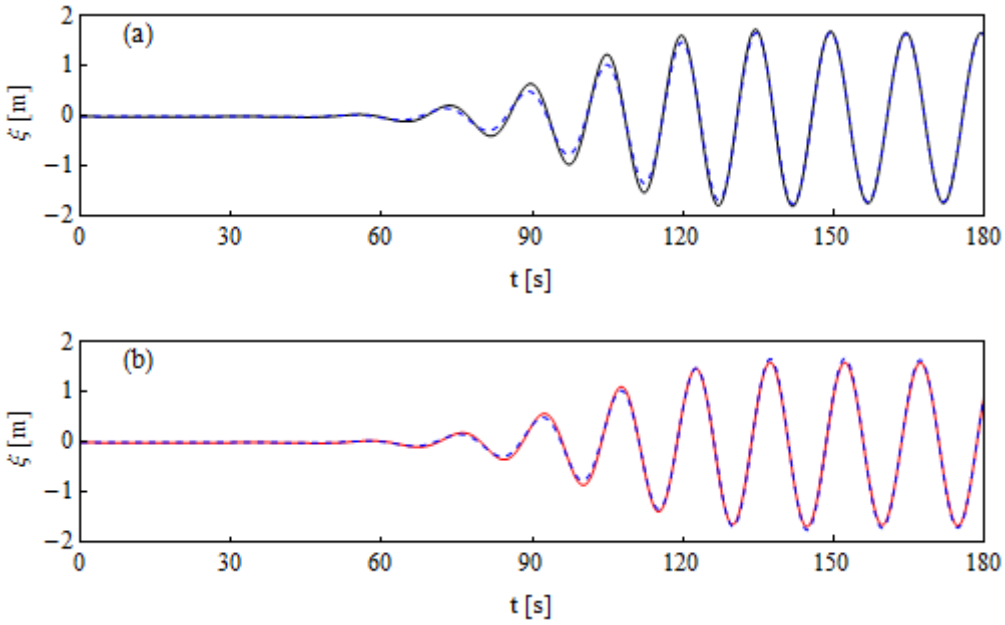

Figure 30: Comparison of the the displacement time-history of device 1 (black) and device 2 (red) in the square array with the displacement time-history of the single device in isolation (dashed blue).

In Figure 30 it is clear that the steady-state displacement oscillations for each device in the square array are almost the same as the phase-shifted signal for the device in isolation. Any discrepancies will become clearer when considering the power take-off where the velocity is squared. The similarity of the behaviour of the devices in the array to a device in isolation can be explained by considering that the parameter $(2\pi/\lambda)r$ at a device spacing of three diameters is sufficiently small to satisfy the point absorber approximation which requires $(2\pi/\lambda)r \ll 1$ (it has been previously observed (Mavrakos & McIver, 1998) that the point absorber theory is valid for $(2\pi/\lambda)r$ values of the order of magnitude of 0.1). Thus, each device in the array creates a small scattered wave relative to the incident wave field which decreases in size as it propagates outward from the structure and only weakly interacts with the other devices. Therefore, the diffracted wave has very little influence on the dynamics of the devices and the devices interact mainly through the radiated waves. However, the radiated waves are relatively small in this case also because the device is not tuned to operate at the resonant frequency and the displacement amplitudes are moderate at less than 2m.

Therefore, the interactions between the devices are relatively weak in that the behaviour of each device is close to that of a device in isolation.

The instantaneous power absorbed from both device 1 and device 2 during the four device simulation is compared to that for the single device in isolation in Figure 31. In this case, the differences between the motions of the devices are magnified by the presence of the velocity squared term. Nevertheless, the power absorbed by device 1 is almost identical to that for the isolated device (apart from a phase shift). However, the power absorbed by device 2 is reduced compared to the single device in isolation by a small fraction – significantly smaller than for the equivalent comparison for the T=9.0s incident wave.

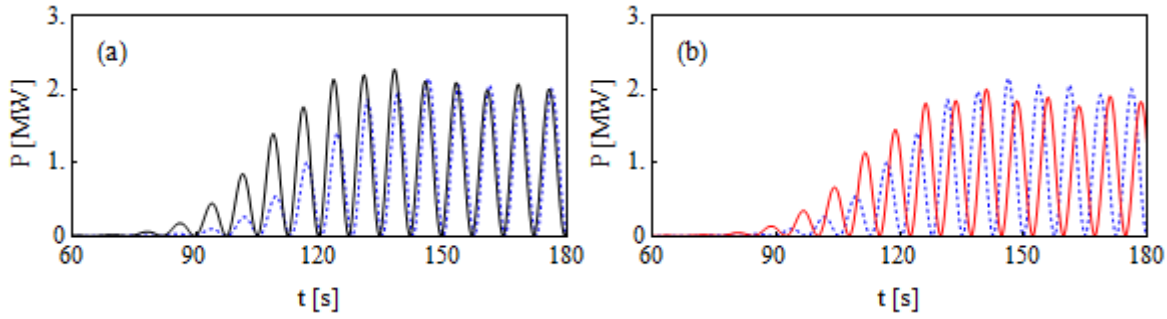

Figure 31: Time-history of the instantaneous power absorbed for (a) device 1 (black) and (b) device 2 (red) compared to the single device in isolation (dashed blue).

Given the similarities in the responses of the devices in the array to the response of the single device in isolation for linear power take off in regular incident waves of period 15s it was deemed unnecessary to investigate the equivalent nonlinear power take-off case because the analysis for the single body would largely be repeated. As a final point, it is worth noting that the power take-off for devices moving without phase control and with optimal amplitude control is twice as large in the case of the 15.0s incident waves as it is for the 9.0s incident waves. To achieve this increase in power take-off a much larger damping force is required for the longer incident wave; however, it illustrates the fact that more energy is available for capture in long waves.

5 CONCLUSIONS

This report presents the results from fully nonlinear simulations of linear and nonlinear power take-off for the controlled heave motion of a single heaving axisymmetric device and the controlled heave motions of a square array of four axisymmetric devices in regular waves. The control of the amplitude of the device motions was achieved by choice of the PTO force coefficient and a number of different approaches to phase control strategies were adopted namely, no phase control, optimal reactive phase control and latching control.

In the OXPOT implementation, the total hydrodynamic force exerted on the bodies is combined with the PTO force (linear or nonlinear) in order to determine the fully nonlinear response of the devices. However, the PTO damping and restoring force coefficients were determined by the linear frequency

domain power absorption theory. Thus, when attempting to optimise the power capture for a given device and incident wave the frequency-domain hydrodynamic coefficients (WG1 WP1 D8 results) were substituted into the optimal amplitude condition (15) and the phase or resonance condition (17). Upon comparing the simulation results for the weakly nonlinear incident waves to the linear frequency-domain predictions in the cases where steady-state was achieved it was found that the predictions of the linear power absorption theory were very close to the weakly nonlinear results. The general principles of the linear power absorption theory are shown to be very useful in understanding the responses and power absorption properties of the devices.

The simulations of the operation of a single device in regular waves can be divided into two broad categories. One set of simulations were run in order to compare the effect of a nonlinear PTO force, in particular the Coulomb damping force that will be used for the QUB experiments in WG2, to a corresponding linear PTO force. In this set of simulations, no phase control was imposed on the motion of the body. However, the other set of simulations modelled both sub-optimal phase control (latching), which approximately satisfies the resonance condition from linear power absorption theory, and optimal phase control which exactly satisfies the resonance condition with the linear PTO only.

The effect of the Coulomb damping force on the device response has been investigated in detail – in each of the comparisons for the T=9.0s incident waves the device responses were quite similar for the linear and equivalent nonlinear PTO forces. The equivalent nonlinear PTO force was determined by taking the RMS value of the linear PTO force at steady state. Although the device responses were found to be quite similar, the instantaneous power extracted by the Coulomb damping PTO force for similar velocity profiles has broader and smaller peaks than the linear damping PTO force. The average linear power take-off was found to be greater in most cases for the linear PTO force. However, in the case of the T=15.0s incident wave the nonlinear power take-off outperformed the linear power take-off. In this case, it was necessary to apply a large Coulomb damping force ($\mu = 2.7MN$ as opposed to the largest value of $\mu = 1.07MN$ in the T=9.0s case) to approximate the effect of the linear damping force at steady state. The effects of the nonlinear PTO force are much more pronounced in this case as is clear from a comparison of the periodic velocity signal with a linear and nonlinear damping force. The amplitude of the velocity is larger for the nonlinear PTO than for the linear PTO thus leading to higher power capture.

In the simulations of devices operating at resonance, the amplitude of the motions were not observed to settle to a steady state, rather they increased throughout the simulation. By applying a stronger PTO damping force, steady state would be reached sooner but the resultant amplitude of the velocity would also be reduced. In the resonant simulations, the instantaneous power absorbed has much larger peak values in resonance than for the case of zero phase control as expected from the linear theory. However, approximate resonance can be observed when latching is implemented for the case where the incident wave period is greater than the natural period of the device. With this suboptimal latching control the same growth of the response amplitude with time was achieved for weak or zero damping. In the comparison between a device without phase control and with latching control for the same linear PTO damping coefficient it was observed that the latched body extracted 60% more power at steady state.

Simulations of the responses and power take-off of four devices in a square array with an inter-device separation along the sides of the square at three diameters were also conducted for incident waves of period 9 seconds and 15 seconds. Both linear and nonlinear power take-offs were implemented and in the case of the T=9.0s incident wave, the devices were also tuned to resonance by specifying the stiffness coefficient to be the value which satisfies the single device resonance condition. In the T=9.0s case, it was observed that the device at the incident wave side of the array reduces the incident wave energy available to the devices behind it through scattering and energy extraction. However, at steady state both device 1 and 2 absorb less energy than the device in isolation for the PTOs and device spacings considered here for the T=9.0s incident wave. In the case of the longer 15.0s period incident waves, weak interactions between the devices were observed with device 1 operating much like the isolated device (given the same PTO damping) and device 2 absorbed slightly less energy but responded in a very similar manner to the isolated device. The similarity in the responses of the array devices to the device in isolation is attributed to the fact that the interaction parameter $(2\pi/\lambda)r$ for the T=15.0s incident wave is approaching the regime of validity of the point absorber approximation.

The number of case studies considered here was relatively restricted, particularly for the square array of four devices. This is a consequence of the long runtimes for the OXPOT simulations whereby a typical runtime on a single processor was approximately 50 hours for the single device simulations and approximately 120 hours for the four device simulations. It is clear that OXPOT is not suitable as a design tool, i.e. a tool for determining optimal PTO coefficients or optimal device configurations in arrays. However, OXPOT is an extremely powerful tool for simulating very complex interactions involving nonlinear free-surface behaviours and complex device motions involving strongly nonlinear applied forces, discontinuous applied forces and device control in addition to the nonlinear hydrodynamic forces.

In the last deliverable (WG1 WP1 D9), we sought to understand and assess the higher order hydrodynamics that OXPOT is capable of simulating. In the present report, however, the focus is on the effect of nonlinearities and discontinuities in the applied PTO forces and control strategies on the response of the devices. The higher order hydrodynamic effects have not been addressed in detail although all solutions include higher order contributions. In later deliverables where validation of the fully nonlinear model against experimental results will be attempted the nonlinear hydrodynamics will be analysed in much more detail in order to compare linear and nonlinear models of the physical interactions involving wave energy devices. In this report, the main source of data available was the frequency-domain coefficients from D8 (as mentioned above) and for this reason no highly nonlinear incident waves were considered.

REFERENCES

Budal, K. & Falnes, J., 1980. Interacting point absorbers with controlled motion. In: *Power from Sea Waves.* London: Academic Press, pp. 381-399.

Clement, A. H. & Babarit, A., 2012. Discrete control of resonant wave energy devices. *Philosophical Transactions of the Royal Society A,* Volume 370, pp. 288-314.

Falnes, J., 2002. *Ocean waves and oscillating systems.* Cambridge: Cambridge University Press.

Falnes, J., 2002. Optimum control of oscillation of wave-energy converters. *International Journal of Offshore and Polar Engineering,* 12(2).

Mavrakos, S. A. & McIver, P., 1998. Comparison of methods for computing hydrodynamic characteristics of arrays of wave power devices. *Applied Ocean Research,* Volume 19, pp. 283-291.

McIver, P., 1994. Some hydrodynamic aspects of arrays of wave-energy devices. *Applied Ocean Research,* Volume 16, pp. 61-69.

Siddorn, P. & Eatock Taylor, R., 2008. Diffraction and independent radiation by an array of floating cylinders.. *Ocean Engineering,* Volume 35, pp. 1289-1303.

Thomas, G. P. & Evans, D. V., 1981. Arrays of three-dimensional wave-energy absorbers. *Journal of Fluid Mechanics,* Volume 108, pp. 67-88.